44. Herrera, P.L. Adult insulin- and glucagon-producing cells differentiate from two independent cell lineages. *Development* **127**, 2317–2322 (2000).
45. Murtaugh, L.C. Pancreas and β-cell development: from the actual to the possible. *Development* **134**, 427–438 (2007).
46. Collombat, P. *et al.* The ectopic expression of Pax4 in the mouse pancreas converts progenitor cells into alpha and subsequently β cells. *Cell* **138**, 449–462 (2009).
47. Thorel, F. *et al.* Conversion of adult pancreatic α-cells to β-cells after extreme β-cell loss. *Nature* **464**, 1149–1154 (2010).
48. Xie, R. *et al.* Dynamic chromatin remodeling mediated by polycomb proteins orchestrates pancreatic differentiation of human embryonic stem cells. *Cell Stem Cell* **12**, 224–237 (2013).
49. Kelly, O.G. *et al.* Cell-surface markers for the isolation of pancreatic cell types derived from human embryonic stem cells. *Nat. Biotechnol.* **29**, 750–756 (2011).
50. Yasunami, Y. *et al.* Vα14 NK T cell-triggered IFN-γ production by Gr-1+CD11b+ cells mediates early graft loss of syngeneic transplanted islets. *J. Exp. Med.* **202**, 913–918 (2005).

Acknowledgments

We thank members of the Gene Technology Center and Center for Animal Resources and Development at Kumamoto University for technical assistance. This work was supported by the Funding Program for Next Generation World-Leading Researchers (to S.K. (no. LS099) and M.U.); the Japan Society for the Promotion of Science, the Realization of Regenerative Medicine (to S.K. and M.U.); the Program for Leading Graduate Schools 'HIGO' (awarded to S.K.); Grants-in-Aid from the Ministry of Education, Culture, Sports, Science and Technology (MEXT), Japan (no. 21390280 to S.K. and no. 22790653 to D. Sakano); and the Collaborative Research Program of Institute for Chemical Research, Kyoto University (grant no. 2010-44). The iCeMS is supported by World Premier International Research Center Initiative, MEXT, Japan.

Author contributions

D. Sakano performed chemical screening, cellular and biochemical analyses; D. Sakano, N.S. and K.U. established the ES cell differentiation system; D. Sakano, K. Kikawa, M.K. and T.Y. performed transplantation assays; K.A. established the ES cell line; S.M., F.E. and N.N. helped maintain AKITA mice; D.M. and M.U. provided and analyzed the chemical library; O.A. and D. Stainier provided chemicals; K. Kume and S.K. provided technical advices, S.K. designed the experiments and wrote the paper. All of the authors discussed the results and commented on the manuscript.

Competing financial interests

The authors declare no competing financial interests.

Additional information

Supplementary information and chemical compound information is available in the online version of the paper. Reprints and permissions information is available online at http://www.nature.com/reprints/index.html. Correspondence and requests for materials should be addressed to S. Kume.

ONLINE METHODS

Ethics statement. This animal work is approved by the Institutional Review Board for Animal Care and Use of Kumamoto University. All animal procedures were conducted according to Kumamoto University guideline.

ES cell lines. The SK7 ES cell line[10] was established from a transgenic mouse line bearing the *Pdx1*-GFP gene. NGP9 ES cells were established by culturing blastocysts obtained from transgenic mice heterozygous for the *Ngn3*-GFP gene[21]. SK7 and NGP9 cells were maintained on MEF feeder cells in Dulbecco's modified Eagle's medium (DMEM; Invitrogen, Carlsbad, CA) supplemented with leukemia inhibitory factor (LIF), 10% FBS, nonessential amino acids (NEAA), L-glutamine (L-Gln), penicillin and streptomycin (PS) and β-mercaptoethanol (β-ME)[10].

Differentiation of ES cells into pancreatic β cells. For differentiation studies, ES cells were plated at 5,000 cells per well, in Corning 96-well plates with Ultra-Web Synthetic Polyamine Surface (no. 3873XX1, Corning Coster, Cambridge, MS). The cells were cultured for 7 d in Medium I: Dulbecco's Modified Eagle Medium (DMEM: Invitrogen, Glasgow, UK) containing 4,500 mg/L glucose and supplemented with 100 μM nonessential amino acids (NEAA), 2 mM L-glutamine (L-Gln; Nacalai tesque, Japan), 1 mM sodium pyruvate (Invitrogen), 50 units/mL penicillin, 50 μg/mL streptomycin (PS; Nacalai tesque), 100 μM β-mercaptoethanol (β-ME; Sigma-Aldrich), ITS (10 μg/mL insulin (Sigma-Aldrich), 5.5 μg/mL transferrin (Sigma-Aldrich) and 6.7 pg/mL selenium (Sigma-Aldrich)), 0.25% Albmax (Invitrogen), 10 ng/ml recombinant human Activin-A (R&D Systems, Minneapolis, MN) and 5 ng/mL recombinant human bFGF (Peprotech). On days 7–11, the cells were cultured in Medium II: RPMI 1640 medium (Invitrogen) containing 2,000 mg/L glucose (Sigma, St. Louis, MO), 1 μM retinoic acid (Sigma-Aldrich), 50 ng/mL human recombinant fibroblast growth factor-10 (human recombinant FGF10, Peprotech, Rocky Hill, NJ), 2% B-27 Supplement (Invitrogen) and 0.25 μM of the Shh signaling antagonist 3-keto-*N*-(aminoethyl-aminocaproyl-dihydrocinnamoyl) cyclopamine (KAAD-cyclopamin, Calbiochem, San Diego, CA). Finally, on days 11–17, cells were cultured in Medium III: DMEM containing 1,000 mg/L glucose supplemented with NEAA, L-Gln, PS, β-ME, ITS, 0.25% Albmax (Invitrogen), 10 nM glucagon-like peptide 1 (GLP-1, Sigma-Aldrich) and 10 mM nicotinamide (NA, Sigma-Aldrich). The medium was replaced every 2 d.

Screening of small molecules and quantitative analysis of imaging. Small molecules from the bioactive, pharmacologically defined Prestwick Chemical Library were screened for pro-differentiation factors. Compounds were dissolved in DMSO (Sigma-Aldrich) and added at 1:100 on day 11, with changes on days 13 and 15. Cells were assayed by immunostaining with mouse anti-insulin (Sigma-Aldrich; I2018; 1:1,000) on day 17. Fluorescent images were quantified by counting pixel numbers representing the number of positive cells, using a ImageXpress Micro scanning system and MetaXpress cellular image analysis software (Molecular Devices, Japan). Data were normalized as fold change relative to DMSO controls. Hit compounds were defined as causing a twofold or higher increase in insulin-positive β cells. Candidate compounds were tested for dose dependency and reproducibility. The screening information is summarized in **Supplementary Table 1**.

Chemicals. Reserpine was purchased from Calbiochem Novabiochem Novagen, TBZ was purchased from Tocris Bioscience, and dibutyryl-cAMP (dBu-cAMP) was purchased from BIOMOL International.

Pargyline was purchased from Cayman Chemicals. The compounds were dissolved in DMSO (final concentration = 1.0%) and added on days 11, 13 and 15. After initial screening, the following concentrations were used: 0.63 μM reserpine, 1.25 μM TBZ, 0.1 μM dopamine (LKT Labs, Inc.), 0.6 μM dBu-cAMP, 1.0 μM pargyline, 1.3 μM α-methyltyrosine (α-MT, Sigma-Aldrich), 0.6 μM L-3,4-dihydroxyphenylalanine (L-DOPA, Toronto Research Chemicals Inc,), 1.3 μM α-fluoromethyl- histidine (α-FMH, Toronto Research Chemicals Inc,), 1.3 μM 5-hydroxy tryptophan (5HTP, Sigma-Aldrich) and 0.6 μM carbachol (Sigma-Aldrich), unless otherwise specified.

Chemical characterization. To confirm the purity of reserpine, TBZ and dBu-cAMP, we checked their HPLC, LC-MS (ESI), and ^{1}H-NMR profiles. The results showed that the reagents we used had high purity (>90%) (**Supplementary Figs. 11–13**). HPLC analysis was performed with a Shimadzu LC-2010C equipped with reversed-phase HPLC column (GL science, Inertsil ODS-3, 4.6 × 150 mm, flow rate 1.0 mL/min, 0.1% TFA CH_3CN/H2O, 10–100%). Mass spectra (ESI) were recorded on a Shimadzu LCMS-2010. ^{1}H-NMR spectra were collected on a JEOL JNM-ECP (300 MHz).

Immunocytochemistry. For immunocytochemistry, ES cells were fixed with 4% paraformaldehyde and processed after 13 days in culture (**Fig. 3** and **Supplementary Fig. 5**), 17 d in culture (**Figs. 1, 2** and **4** and **Supplementary Fig. 6**) or 6 weeks after transplantation (**Supplementary Fig. 10**). For examination of target protein expression in single cells, ES cell–derived differentiated cells were dissociated with 0.25% trypsin (Invitrogen), replated for 30 min and then fixed and processed for immunocytochemistry. The following antibodies were used: rabbit anti-MafA (Abcam; ab17976; 1/100,), rabbit anti–C-peptide (Cell Signaling; 4593, 1/100), guinea pig anti-insulin (Dako; A0564; 1/1,000), rabbit anti-pancreatic polypeptide (Dako; A619; 1/100), mouse anti-Nkx2.2 (Developmental Studies Hybridoma Bank, University of Iowa; 74.5A5; 1/100), mouse anti-Nkx6.1 (Developmental Studies Hybridoma Bank, University of Iowa; F64A6B4; 1/100), rabbit anti-GFP (MBL International Corp; 598; 1/1,000), goat anti-Pdx1 (R&D systems; AF2419, 1/100), goat anti-amylase (Santa Cruz Biotechnology; sc-12821; 1/100), goat anti-somatostatin (Santa Cruz Biotechnology; sc-7819; 1/100), mouse anti-glucagon (Sigma-Aldrich; G2654; 1/1,000), biotin-conjugated *D. biflorus* agglutinin (DBA) lectin (Sigma-Aldrich; L6533; 1/500) and mouse anti-insulin (Sigma-Aldrich; I2018; 1/1,000) antibodies were used. Secondary antibodies used were Alexa 488–conjugated goat anti-mouse IgG (A11029; 1/1,000), Alexa 568–conjugated goat anti-guinea pig IgG (A11075; 1/1,000), Alexa 568–conjugated goat anti-mouse IgG (A11031; 1/1,000), Alexa 568–conjugated goat anti-rabbit IgG (A11036; 1/1,000), Alexa 568–conjugated anti-streptabidine antibody (S11223; 1/1,000), or Alexa 633–conjugated donkey anti-goat IgG (A21082; 1/1,000), Alexa 633–conjugated goat anti-mouse IgG (A21053; 1/1,000), Alexa 633–conjugated goat anti-rabbit IgG (A21072; 1/1,000) (all from Invitrogen). Cells were counter-stained with DAPI (Roche Diagnotics, Basel, Switzerland).

Gene silencing. In the VMAT2-knockdown assays, cells were transfected with Expression Arrest nonsilencing, control shRNA (Open Biosystems, no. RHS4080), VMAT2 shRNA (Open Biosystems, no. RMM3981-97058457 and no. RMM3981-97058458). The lentiviral vectors were constructed as previously described[11]. SK7 cells were infected with viral supernatants. After 24 h of incubation, the virus-containing medium was replaced with fresh ES maintenance medium. After 24 h of incubation, infected cells were selected using 1.5 μg/mL puromycin (Sigma-Aldrich). The surviving cells were harvested, and clones were selected to establish knockdown and control cell lines.

Measurement of intracellular monoamine levels. Cells were treated with chemicals before harvest (days 11–17). Cells were lysed with lysis buffer containing 0.1% Triton X-100 (Nakarai Tesque, Japan) in 0.1 M PBS (pH7.2, Sigma-Aldrich) with protease inhibitor cocktail. Lysates were assayed for dopamine, histamine, serotonin, adrenaline or noradrenaline with each monoamine-specific ELISA kit (Labor Diagnostika Nord GmbH & Co.; KG Nordhorn Germany).

EdU incorporation. Cells were treated with culture medium containing 20 μM 5-ethynyl-2′-deoxyuridine (EdU) for 48 h before harvest (days 17–19), processed using the Click-iT EdU Alexa Fluor 594 Imaging Kit (Invitrogen) and stained with DAPI and anti-GFP antibodies, rabbit anti-GFP (no. 598; 1:1,000; MBL International Corp., Woburn, MA) and detected with Alexa 488-conjugated goat anti-rabbit IgG (Invitrogen; A-11008; 1:1,000).

Pancreas bud *in vitro* culture. Pancreas buds were dissected from E12.5 embryos of a transgenic mouse line bearing the *Pdx1*- green fluorescent protein (GFP) gene. The tissue was placed onto 12-well Corning Transwell cell culture inserts (Corning Coster, Cambridge, MS). The bottom of the inserts were touched with medium containing M199 with NEAA, L-Gln, PS, β-ME and 10% FBS (FBS, Hyclone).

Flow cytometry. Cells were collected and suspended in 1 × HANKS with 1% FBS. A FACS Aria II flow cytometry cell sorter (Becton Dickinson Immunocytometry Systems, San Jose, CA) was used to purify GFP-positive cells by sorting them against the fluorescence profiles of differentiating cells prepared from wild-type mice. Dead cells were identified using propidium iodide (Sigma-Aldrich).

Quantitative real-time PCR. RNA was extracted from ES cells, mouse tissue or transplanted grafts using the RNeasy minikit (Qiagen, Hilden, Germany) and then treated with DNase I (Qiagen).

Complementary DNA was synthesized from 1 μg of total RNA using Revertra Ace qPCR RT Master Mix (Toyobo).

For real-time PCR analysis, the mRNA expression was quantified with SyberGreen on an ABI 7500 thermal cycler (Applied Biosystems, Foster City, CA). The level of expression of each gene was normalized with that of the β-actin–expressing gene *Actb* . The PCR conditions were as follows: denaturation at 95 °C for 15 s, annealing and extension at 60 °C for 60 s for up to 40 cycles. Each measurement was normalized to *Actb* (mouse) expression for each sample by subtracting the average *Actb* (mouse) expression. C_t values (threshold cycle) from the average Each gene C_t, resulting in C_t Target mRNA levels are expressed as arbitrary units. All of the primers for real-time PCR are listed in **Supplementary Table 2**.

Measurement of glucose-stimulated C-peptide secretion and cellular or plasma C-peptide level by enzyme-linked immunosorbent assay. Differentiating ES cells were preincubated for 0.5 h in low glucose (5.5 mM) DMEM with minimal essential medium and 1% FBS. Cells were washed twice with phosphate-buffered saline then incubated for 2 h in low-glucose (5.5 mM) or high-glucose (27.5 mM) DMEM with 1% FBS. The culture medium was collected, and cells were lysed with a lysis buffer of 0.1% Triton X-100 in PBS with added protease inhibitor cocktail. Insulin secretion into the culture medium and insulin content of the cell lysates were measured using a mouse C-peptide ELISA kit (Shibayagi Co. Ltd., Japan).

IPGTT. Mice fasted for 16–18 h were used. Body weights were measured. Blood glucose levels were measured before (0 min) or at 15 min, 30 min, 60 min, 90 min and 120 min after intraperitoneal administration of 25% Glucose (Sigma-Aldrich) solution at 2 g per kg body weight. Serum C-peptide concentrations were measured as described above.

Cell transplantation into AKITA mice. Differentiated cells were dissociated with 0.25% trypsin, resuspended in DMEM with 10% FBS and injected under the kidney capsules of AKITA mice (C57BL/6J-*Rag1*$^{-/-}$*Ins2*$^{Akita/+}$; male)[27] with a 24G catheter (NIPRO, Japan). The AKITA mice were at least 6 weeks old. Six weeks after transplantation, the tissue was removed and analyzed for insulin expression, content and secretion, as described above.

Statistical tests. Data were analyzed by two-tailed *t*-test. Data are presented as mean ± s.d.

doi:10.1038/nchembio.1410

Cell Stem Cell
Article

Redefining the In Vivo Origin of Metanephric Nephron Progenitors Enables Generation of Complex Kidney Structures from Pluripotent Stem Cells

Atsuhiro Taguchi,[1] Yusuke Kaku,[1] Tomoko Ohmori,[1] Sazia Sharmin,[1] Minetaro Ogawa,[2,3] Hiroshi Sasaki,[4] and Ryuichi Nishinakamura[1,3,*]
[1]Department of Kidney Development, Institute of Molecular Embryology and Genetics, Kumamoto University, 2-2-1 Honjo, Kumamoto 860-0811, Japan
[2]Department of Cell Differentiation, Institute of Molecular Embryology and Genetics, Kumamoto University, 2-2-1 Honjo, Kumamoto 860-0811, Japan
[3]Japan Science and Technology Agency, CREST, 2-2-1 Honjo, Kumamoto 860-0811, Japan
[4]Department of Cell Fate Control, Institute of Molecular Embryology and Genetics, Kumamoto University, 2-2-1 Honjo, Kumamoto 860-0811, Japan
*Correspondence: ryuichi@kumamoto-u.ac.jp
http://dx.doi.org/10.1016/j.stem.2013.11.010

SUMMARY

Recapitulating three-dimensional (3D) structures of complex organs, such as the kidney, from pluripotent stem cells (PSCs) is a major challenge. Here, we define the developmental origins of the metanephric mesenchyme (MM), which generates most kidney components. Unexpectedly, we find that posteriorly located T^+ MM precursors are developmentally distinct from $Osr1^+$ ureteric bud progenitors during the postgastrulation stage, and we identify phasic Wnt stimulation and stage-specific growth factor addition as molecular cues that promote their development into the MM. We then use this information to derive MM from PSCs. These progenitors reconstitute the 3D structures of the kidney in vitro, including glomeruli with podocytes and renal tubules with proximal and distal regions and clear lumina. Furthermore, the glomeruli are efficiently vascularized upon transplantation. Thus, by reevaluating the developmental origins of metanephric progenitors, we have provided key insights into kidney specification in vivo and taken important steps toward kidney organogenesis in vitro.

INTRODUCTION

Despite the successful achievement of various types of tissues from pluripotent stem cells (PSCs), kidney generation in vitro has remained a challenge for developmental biology and regenerative medicine (Murry and Keller, 2008; Williams et al., 2012). This is partly because the specification of the kidney lineage in vivo has not been well clarified, owing to its complex processes involving the formation of three consecutive primordia (pronephros, mesonephros, and metanephros) during embryogenesis (Saxen, 1987). The pronephros and mesonephros eventually degenerate in females, whereas a portion of the mesonephros in males contributes to a drainage system for the future testis, including the epididymis. The kidney derives from the embryonic metanephros, which develops at the most posterior part of the body trunk. The metanephros is formed by reciprocally inductive interactions between two precursor tissues, namely the metanephric mesenchyme (MM) and the ureteric bud. Cell fate analyses have shown that both the MM and ureteric bud derive from the intermediate mesoderm, which appears around embryonic day 8.5 (E8.5) and expresses the transcription factor *Osr1* (Mugford et al., 2008b). However, the mechanisms underlying how the nascent mesoderm becomes committed to the intermediate mesoderm and how the MM and ureteric bud lineage segregate from one another have not been clarified, despite many reports showing the importance of various growth factors during kidney development (Costantini and Kopan, 2010; Fleming et al., 2013; Kim and Dressler, 2005; Moriya et al., 1993; Poladia et al., 2006). Moreover, it remains to be elucidated how the anteroposterior axis is formed along the intermediate mesoderm and gives rise to the posteriorly located metanephros. In the present study, we addressed these questions by in vivo lineage-tracing experiments together with in-vitro-directed differentiation systems utilizing sorted embryonic kidney precursors at each developmental stage. Importantly, by establishing conditions for the later stages first, and then moving backward to the earlier stages, we were able to optimize the multistep culture conditions from embryonic precursors toward nephron progenitors. Finally, the protocol established by these strategies was successfully applied to the induction of metanephric nephron progenitors from mouse embryonic stem cells (ESCs) and human induced pluripotent stem cells (iPSCs), thereby advocating a model for kidney lineage specification.

RESULTS

The $Osr1^+$/Integrina8$^+$/$Pdgfra^-$ Population Represents Colony-Forming Nephron Progenitors

The MM gives rise to the epithelia of glomeruli (i.e., podocytes) and renal tubules, which constitute the major parts of the nephrons, as shown by cell fate analyses involving labeling of

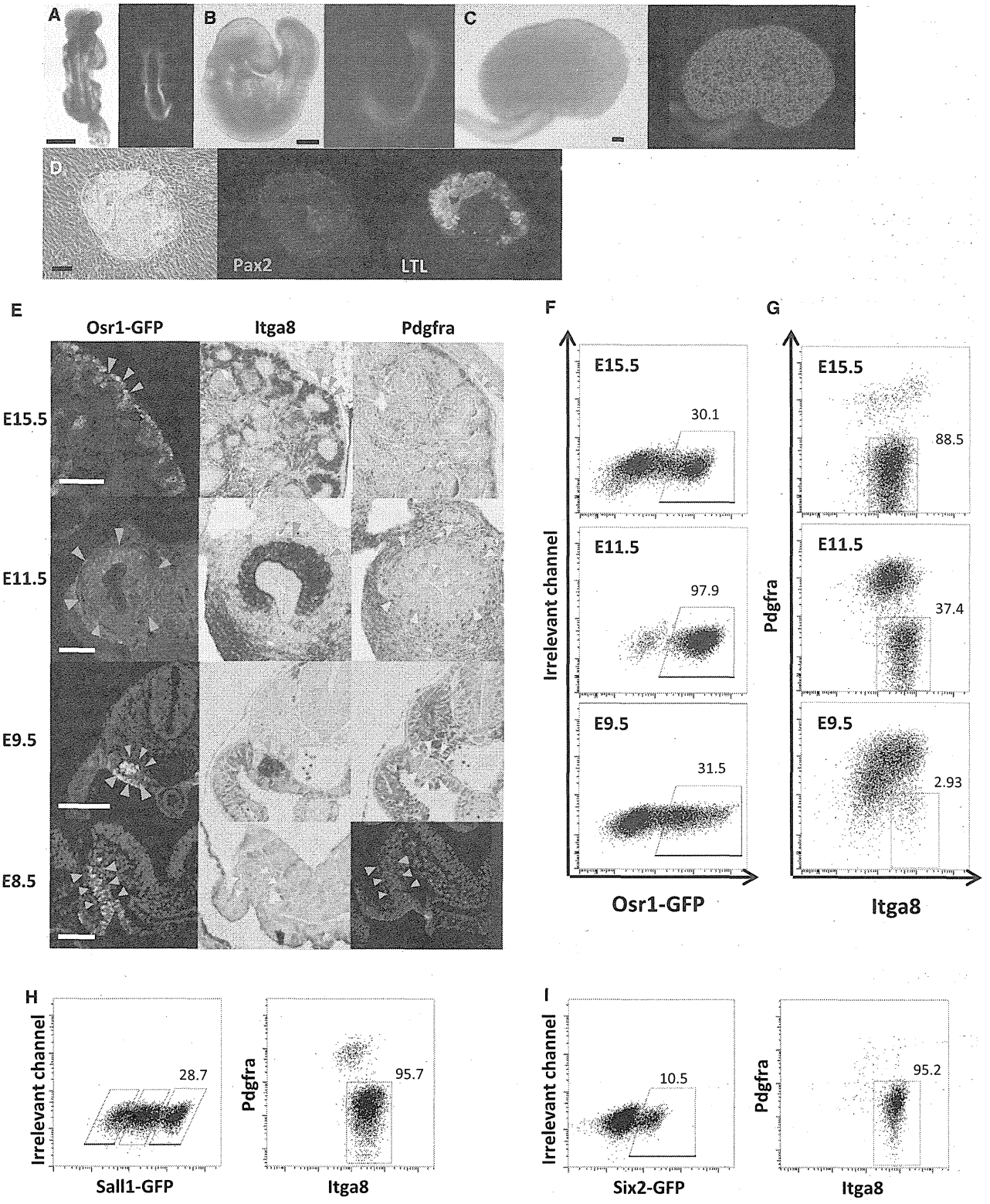

Figure 1. Nephron Progenitors Exist in the Osr1$^+$/Itga8$^+$/Pdgfra$^-$ Population

(A–C) EGFP expressions in Osr1-GFP knockin mice at E8.5 (A), E9.5 (B), and E15.5(C) are shown. Scale bars, 500 μm.

(D) Bright-field image and immunostaining of a colony are presented. Scale bar, 100 μm.

(legend continued on next page)

mesenchyme expressing the transcription factor *Six2* (Kobayashi et al., 2008). We previously proved the presence of nephron progenitors by establishing a colony-formation assay. When we plated dissociated metanephric mesenchymal cells, which strongly express *Sall1*, onto feeder cells stably expressing *Wnt4*, single cells formed colonies that expressed glomerular and renal tubule markers (Nishinakamura et al., 2001; Osafune et al., 2006). Therefore, the Sall1^{high} and Six2^{+} MM represents a nephron progenitor population in the embryonic kidney.

Osr1 is another MM marker and also one of the earliest markers for the intermediate mesoderm and is thus continuously expressed in the renal precursor population throughout kidney development (James et al., 2006; Mugford et al., 2008b). We generated Osr1-GFP knockin mice (Figures S1A–S1C available online) and confirmed that GFP was expressed in the intermediate mesoderm at E8.5–E9.5 and the MM at E11.5–E15.5 (Figures 1A–1C). Similar to our previous experiments, the Osr1-GFP^{+} population sorted from E11.5 and E15.5 embryonic kidneys contained colony-forming nephron progenitors (Table S1). The colonies expressed nephric transcription factors, such as *Pax2* and *Sall1*, as well as markers for differentiated renal tubules (Figures 1D and S1D). Therefore, the Osr1^{+} MM contains colony-forming nephron progenitors.

Next, we searched for cell surface markers that can further enrich the nephron progenitors. At E15.5 and E11.5, Integrina8 (Itga8) was strongly expressed in the capping mesenchyme around the ureteric bud tips, whereas Pdgfra was excluded from the population (Li et al., 2000; Müller et al., 1997) (Figure 1E). By fluorescence-activated cell sorting (FACS) analyses, we identified the existence of Itga8^{+}/Pdgfra^{-} fractions in the Osr1-GFP^{+} populations of E15.5 and E11.5 embryonic kidneys (Figures 1F and 1G), and colony-forming nephron progenitors were enriched in the Osr1^{+}/Itga8^{+}/Pdgfra^{-} fractions (Table S2). It is of note that not all cells in the Itga8^{+}/Pdgfra^{-} fraction of each specimen were positive for Osr1-GFP, meaning that all three markers were required for identification of the nephron progenitor populations (Figure S1E). We further confirmed the reliability of these cell surface markers using *GFP* knockin mice for *Sall1* and *Six2*, in which most of the Sall1-GFP^{high} or Six2-GFP^{+} cells were Itga8^{+}/Pdgfra^{-} (Figures 1H and 1I). Therefore, the Osr1-GFP^{+}/Itga8^{+}/Pdgfra^{-} fraction represents the colony-forming nephron progenitors.

The Anterior Intermediate Mesoderm at E9.5 Contains Colony-Forming Progenitors that Contribute to the Mesonephros

We next examined the expressions of nephron progenitor markers and the colony-forming abilities of Osr1-GFP^{+} cells at earlier stages. At E8.5, we did not detect any overlap of GFP with Itga8, and no colonies were formed by the GFP^{+} population (Figure 1E; Table S1). At E9.5, we detected colony formation by the GFP^{+} population (0.037% ± 0.013%; Table S1; Figures S2A and S2B). We also found a GFP^{+} region that was Itga8^{+}/Pdgfra^{-} (Figure 1E), and sorting of the Osr1^{+}/Itga8^{+}/Pdgfra^{-} population enriched the colony-forming cells (1.10% ± 0.26%; Figures 1F and 1G; Table S2). However, even after the enrichment, the colony-forming frequency was significantly lower than those of the Osr1^{+}/Itga8^{+}/Pdgfra^{-} populations from the metanephric region at E10.5 and E11.5 (30.9% ± 1.5% and 50.9% ± 5.2%, respectively; Table S2). In contrast, the colony-forming frequency of the Osr1^{+}/Itga8^{+}/Pdgfra^{-} population from the mesonephric region at E10.5 (1.47% ± 0.20%) was as low as that from E9.5. Because the mesonephros, which is located anterior to the metanephros, develops earlier than the metanephros and forms much fewer nephrons (Saxen, 1987), we hypothesized that the colony-forming cells at E9.5 may represent mesonephric nephron progenitors. Indeed, colony-forming progenitors were only detected among the anterior part of GFP^{+} cells in the E9.5 embryo (Figure S2C). Furthermore, Pax2 and Six2, which mark nephron progenitors, were predominantly expressed in the anterior part of the intermediate mesoderm (Figure 2A). We further crossed *Six2-GFPCreER* mice (Kobayashi et al., 2008) with mice carrying a *tdTomato* reporter allele (Madisen et al., 2010) and injected tamoxifen to transiently activate Cre in the anterior intermediate mesoderm at E9.5. When analyzed at E11.5, labeled cells were detected in the mesonephros, but not in the metanephros (Figure S2D). Therefore, the anterior and posterior parts of the Osr1-GFP^{+} intermediate mesoderm at E9.5 have different characteristics, and the anterior intermediate mesoderm, which contributes to the mesonephros, may not give rise to the metanephric nephron progenitors.

Metanephric Nephron Progenitor Induction from the Posterior Intermediate Mesoderm at E9.5

To further investigate the molecular differences and required factors between the early stages of kidney precursor development, we performed microarray and quantitative RT-PCR analyses using the Osr1^{+}/Itga8^{+}/Pdgfra^{-} colony-forming presumptive mesonephric progenitors at E9.5 and metanephric nephron progenitors at E10.5–E11.5 (Figures 2B and S3A). Although both types of progenitors expressed many transcriptional factors in common, such as *Osr1*, *Wt1*, *Pax2*, and *Six2*, the metanephric progenitors expressed posterior *Hox* genes including *Hoxa10*, *Hoxa11*, and *Hoxd12* more abundantly. The *Hox11* family genes, which start to be expressed at the posterior end of the embryo around E9.0, are essential for metanephros development by dictating the metanephric region along the anterior-posterior axis in the intermediate mesoderm (Mugford et al., 2008a; Nelson et al., 2008; Wellik et al., 2002). Furthermore, a cell fate-mapping study showed that the Osr1^{+} intermediate mesoderm at E9.5 contributes to the MM (Mugford et al., 2008b). Therefore, we hypothesized that the non-colony-forming *Osr1*$^{+}$/*Wt1*$^{+}$/*Pax2*$^{-}$/*Six2*$^{-}$/*posterior*

(E) Immunostaining of embryonic sections is shown. Red color staining shows the CK8 expression in the ureteric bud (E15.5). The arrowheads indicate the capping mesenchyme at E15.5 and E11.5, condensed intermediate mesoderm at E9.5, and intermediate mesoderm at E8.5. Scale bars, 100 μm.
(F and G) FACS analyses of Osr-GFP (F) and Itga8/Pdgfra (G) in the embryos at each indicated stage are shown.
(H and I) FACS analyses of the Sall1-GFP^{high} population (H) and Six2-GFP^{+} population (I) in the E11.5 metanephros and of Itga8/Pdgfra expressions are presented.
See also Figures S1 and S2, and Tables S1 and S2.

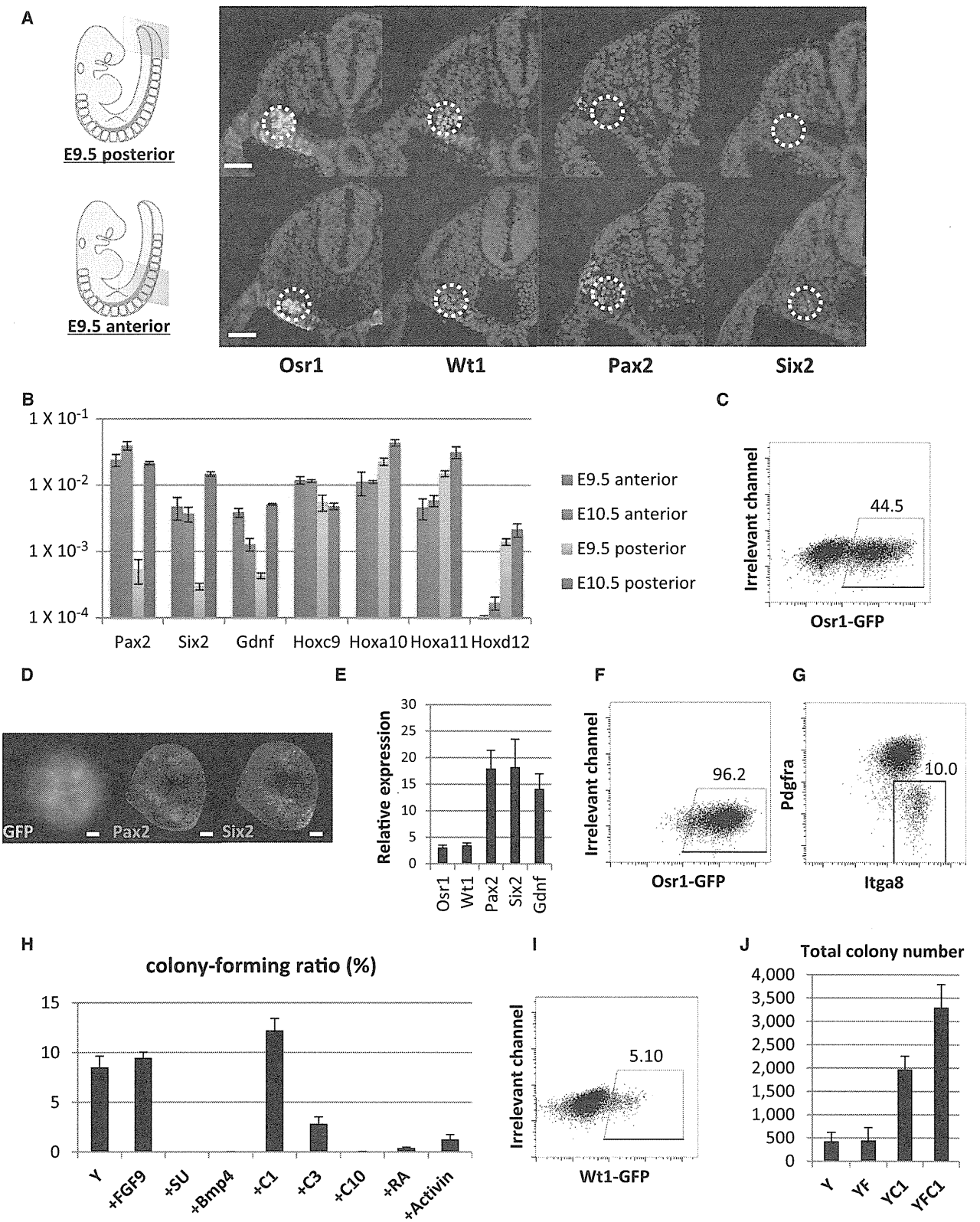

(legend on next page)

Hox$^+$ intermediate mesoderm, which was located posteriorly at E9.5, could be a precursor population for the metanephric nephron progenitors.

To test our hypothesis, we sorted Osr1-GFP$^+$ cells from the posterior part of E9.5 embryos and plated them into low-cell-binding plates in the presence of the Rho kinase inhibitor Y27632, which supports cell survival (Watanabe et al., 2007) (Figures 2C and S3B). The cells spontaneously reaggregated and formed spheres within 24 hr. At 48 hr of culture, the aggregates retained intense GFP signals and showed more than 10-fold higher expressions of *Pax2*, *Six2*, and *Gdnf* compared with the starting point (Figures 2D–2F). FACS analyses also showed the emergence of an Osr1$^+$/Itga8$^+$/Pdgfra$^-$ population (10.0% ± 0.01% of the total cells; Figures S3C and 2G). When these aggregates were dissociated and stimulated with Wnt4, colony formation was observed (Figure 2H), suggesting in vitro derivation of metanephric nephron progenitors from the posterior intermediate mesoderm.

We further addressed the effects of growth factors in this process. The microarray data described above showed the accumulated expressions of Fgf ligands (especially *Fgf9* and *Fgf20*), receptors, and their downstream target genes in the colony-forming populations at both E9.5 and E11.5, whereas the Bmp and Wnt targets were downregulated (Figure S4A). Indeed, inhibition of Fgf signaling, exogenous addition of Bmp4, or high concentrations of a Wnt agonist (3 or 10 μM CHIR99021 [CHIR]), as well as addition of retinoic acid or activin, were inhibitory for the induction of colony-forming progenitors and nephric gene expressions (Figures 2H and S4B), whereas addition of FGF9 or a low concentration of the Wnt agonist (1 μM CHIR) slightly improved the colony formation (Figure 2H). Because Osr1-GFP is expressed by a rather broad population, including the lateral plate mesoderm, we examined the efficacy of these factors using *Wt1-GFP* knockin mice (Zhou et al., 2008), which show more restricted expression in a region of the intermediate mesoderm (Figures 2A, 2C, and 2I). Addition of Fgf9 and a low dose of the Wnt agonist synergistically promoted sphere growth and increased colony formation by the spheres (Figures 2J and S4C).

Thus, the combination of 1 μM CHIR and Fgf9 (C1F) was optimal for induction of metanephric nephron progenitors from the posterior intermediate mesoderm. These observations are consistent with previous findings showing requirements of Fgf receptors and Fgf9/Fgf20 for the formation and maintenance of the MM, respectively (Barak et al., 2012; Poladia et al., 2006).

The Precursor of the MM Is Maintained in the T$^+$ Caudal Population until the E8.5 Postgastrulation Stage

Next, we searched for an in vitro method to differentiate the mesoderm at earlier stages into MM by way of the E9.5 posterior intermediate mesoderm. One report has shown that both the MM and ureteric bud derive from the intermediate mesoderm, which appears around E8.5 and expresses *Osr1* (Mugford et al., 2008b). Several other reports have shown that the ureteric bud originates from the anterior intermediate mesoderm, and its anlage, the Wolffian duct, elongates in an anterior-to-posterior manner, as demonstrated by direct labeling in chick embryos (Atsuta et al., 2013; Attia et al., 2012; Obara-Ishihara et al., 1999; Saxen, 1987). In murine embryos, the Pax2$^+$/Pax8$^+$ anterior intermediate mesoderm at E8.5, called the pronephric anlage, is supposed to be the equivalent population (Bouchard et al., 2002) and is included in the Osr1$^+$ region. Thus, we initially examined the effects of many combinations of growth factors on sorted E8.5 Osr1-GFP$^+$ cells. However, we were unable to induce colony-forming progenitors. Unexpectedly, we experienced colony formation from the Osr1-GFP$^-$ fraction when treated with growth factors. Therefore, we hypothesized that the posterior immature mesoderm, which was negative for Osr1, contained prospective nephron progenitors. Deletion of *T* (*Brachyury*), a representative marker of the primitive streak and posterior nascent mesoderm, causes a caudal truncation that includes the metanephric region (Herrmann et al., 1990). We first crossed *T$^{nEGFP\text{-}CreERT2/+}$* mice (Imuta et al., 2013) with mice carrying the *tdTomato* reporter allele and injected tamoxifen at the gastrulation stage (E6.5 and E7.5), when the initial germ layer formation takes place (Murry and Keller, 2008; Tam and Behringer, 1997). When analyzed at E11.5, most of the mesodermal tissues, including the heart, limbs, and kidneys, were labeled (Figures 3A and 3B). Next, we injected tamoxifen at E8.5 and found that labeled cells were only detected in the lower trunk of the E11.5 embryo, including the MM located at the hindlimb level (Figure 3A). On the other hand, the heart and forelimbs, which are anteriorly located mesodermal tissues, were no longer labeled (Figure 3A). Surprisingly, when we created sections at the metanephric level, only the MM, and not the ureteric bud, was labeled (Figure 3B). These findings indicate that at E8.5, the precursor of the ureteric bud was located anteriorly in the T$^-$ population and already segregated from that of the MM, which was localized in T$^+$ posterior nascent mesoderm. These data are consistent with the notion that the ureteric bud originates from the anterior intermediate mesoderm at E8.5 and

Figure 2. Metanephric Nephron Progenitor Induction from the E9.5 Posterior Intermediate Mesoderm

(A) Immunostaining for the indicated regions is presented. The intermediate mesoderm is outlined by the dashed lines. Scale bars, 50 μm.

(B) E9.5 and E10.5 anterior are the mesonephric progenitors, E10.5 posterior is the metanephric progenitors, and E9.5 posterior is the caudal intermediate mesoderm. The relative expression of each transcript to β-actin expression is presented as the mean ± SEM (n = 3).

(C) Osr1-GFP$^+$ population gated for cell sorting is shown.

(D) GFP and immunostaining of cultured cell aggregates are shown. Scale bars, 100 μm.

(E) Relative expression of each transcript to the starting material is presented as the mean ± SEM (n = 3).

(F and G) FACS analyses of Osr1-GFP expression (F) and Itga8/Pdgfra expression (G) are shown.

(H) Colony-forming ratios of cultured cell aggregates are presented as the mean ± SEM (n = 3). Y, Y27632 (Rock inhibitor); SU, SU5402 (Fgfr1 inhibitor); C1, 1 μM CHIR (canonical Wnt agonist); C3, 3 μM CHIR; C10, 10 μM CHIR, RA, retinoic acid.

(I) Wt1-GFP$^+$ population gated for cell sorting is shown.

(J) Total colony numbers from cultured cell aggregates are presented as the mean ± SEM (n = 5). F, Fgf9.

See also Figures S2–S4.

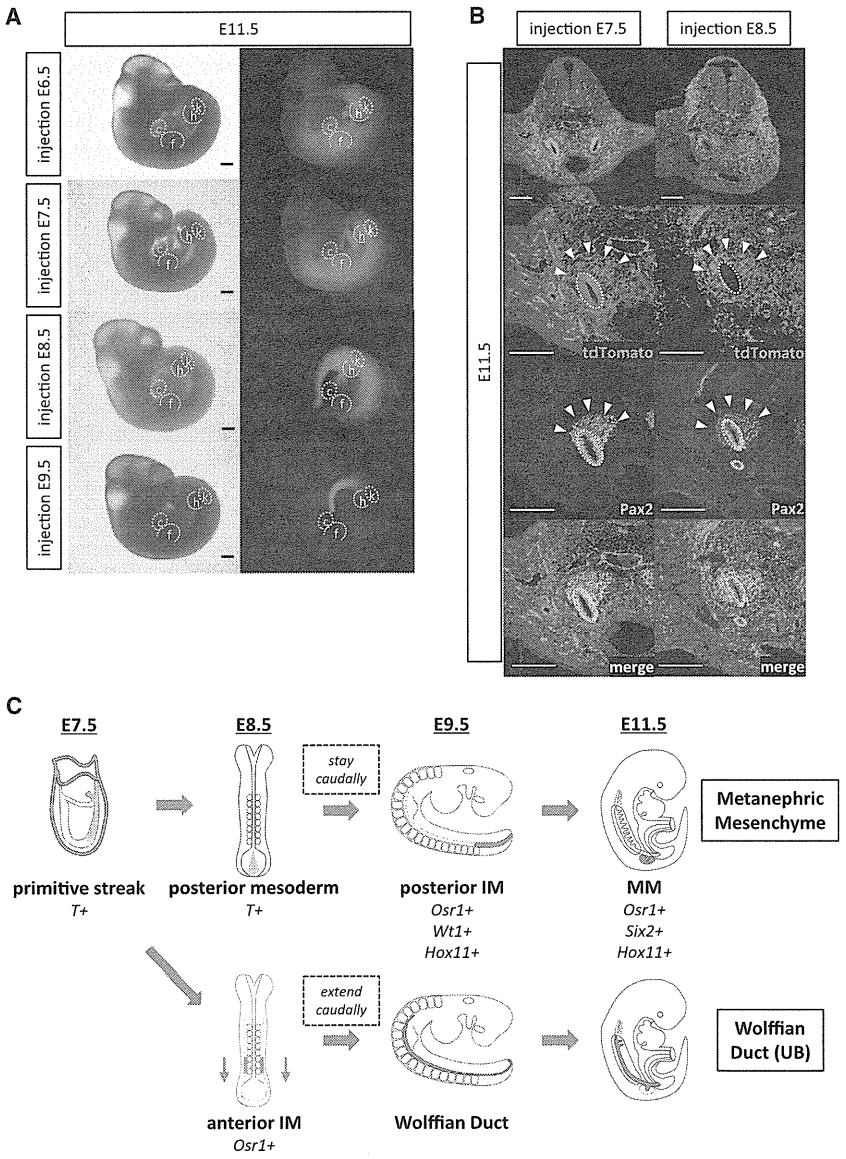

Figure 3. The MM Is Derived from the Posterior Mesoderm Maintained in the T$^+$ Nascent State until E8.5

(A) Lateral view shows E11.5 whole embryos (left panels) and comparisons of fluorescent labeling after injection of tamoxifen at various stages. The regions of the heart (c), metanephric kidney (k), forelimb (f), and hindlimb (h) are indicated by dashed lines. Scale bars, 500 μm.

(B) Immunostaining of an E11.5 embryo labeled by injections of tamoxifen at E7.5 and E8.5 is shown. The arrowheads indicate the MM, and the ureteric buds are outlined by dashed lines. Scale bars, 100 μm.

(C) Model for lineage segregation of the ureteric bud (UB) and the MM is shown. IM, intermediate mesoderm.

See also Figure S5.

elongates caudally (Figure 3C). In contrast, when we injected tamoxifen at E9.5, only the tail region was labeled, and no labeled cells were observed in the MM region (Figure 3A), suggesting that the T$^+$ cells at this stage no longer possess the capacity to differentiate into the MM.

Taken together, our observations indicate that the precursor of the MM is maintained and posteriorized in the T$^+$ state until the E8.5 postgastrulation stage (Figure 3C). Presumably, this could in part correspond to the "axial progenitor," which was recently recognized as the source of the caudal body trunk (Wilson et al., 2009). These data also reveal differences in the developmental processes between the posteriorly located MM and the anteriorly located mesodermal tissues, such as the heart, which have been successfully induced from PSCs by way of the T$^+$ state in the initial short period of differentiation (Burridge et al., 2012).

MM Induction from the T$^+$ Caudal Precursor at E8.5

Based on the lineage-tracing experiments, we used the sorted E8.5 T$^+$ posterior mesoderm as the starting material to induce metanephric nephron progenitors (Figures 4A–4C). The sorted cells were reaggregated to form spheres and treated with various growth factors, followed by treatment with C1F as described above (Figure 4C, step 3). Because the posterior intermediate mesoderm in E9.5 embryo was marked by expressions of *Osr1*, *Wt1*, and posterior *Hox* genes, we first focused on the growth factors that may affect the expressions of these genes. Synergistic effects of Bmp and Wnt signaling have been reported on the expressions of posterior *Hox* genes in mouse ESC differentiation (Lengerke et al., 2008), and retinoic acid signaling is important for the expressions of *Wt1* homologs in zebrafish development (Bollig et al., 2009). Because simultaneous introduction of retinoic acid, Bmp, and the Wnt agonist did not increase the posterior *Hox* genes to the levels observed in the embryonic MM (Figures 4D and 4E), we added a "posteriorization phase." Because canonical Wnt signals are reportedly important for caudal body extension (Wilson et al., 2009; Yamaguchi et al., 1999), we added a high concentration of the Wnt agonist (10 μM CHIR) in combination with Bmp4. This treatment (Figure 4C, BC10 in step 1) dramatically increased the expressions of posterior *Hox* genes, and we were able to detect colony formation from the induced cells, although the expression levels of nephric genes were still lower than those in the embryonic MM (Figures 4D–4G). We tried various conditions and found that the combination of activin and retinoic acid, together with Bmp4 and 3 μM CHIR (Figure 4C, ABC3 in; step 2), substantially increased the expressions of nephric genes (Figure 4F). In this optimized three-step condition (BC10 followed by ABC3R and C1F), the

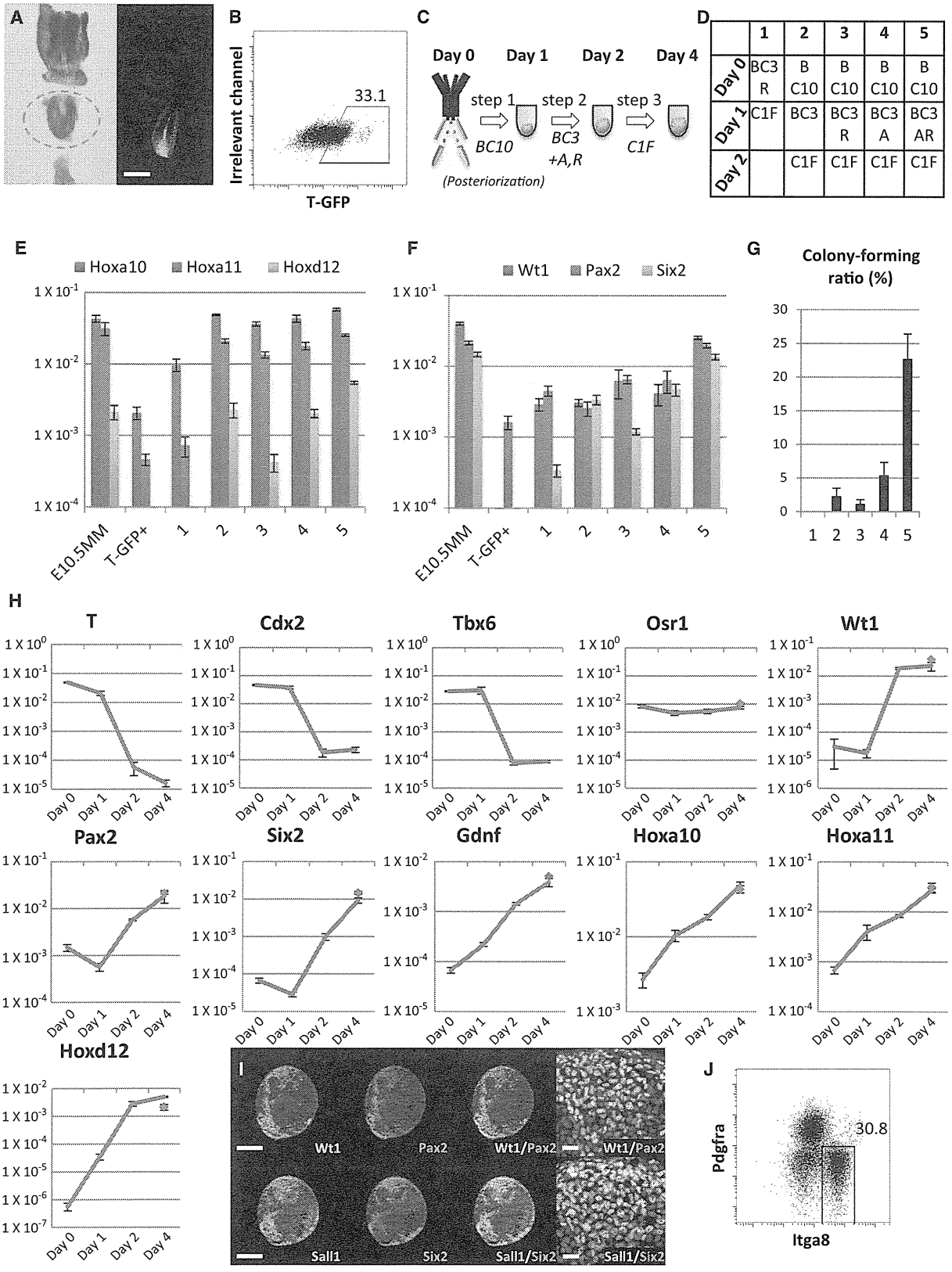

(legend on next page)

cells formed higher numbers of colonies (22.7% ± 3.66%, n = 4) compared with single addition of either activin or retinoic acid (Figure 4G). In the first posteriorization step, the concentration of the canonical Wnt agonist was critically important, and addition of retinoic acid completely inhibited the colony-forming progenitor induction (Figure S5A). In the second step, inhibition of any one of activin, retinoic acid, Bmp, Wnt, or Fgf signaling resulted in a decrease in colony formation (Figure S5B), suggesting that all of these signals were essential. We further examined the temporal kinetics of the gene expressions at every step of the induction process (Figure 4H). In the first step, *T*, *Cdx2*, and *Tbx6*, all of which are posterior nascent mesoderm markers, were expressed and maintained, whereas posterior *Hox* genes started to increase. In the second step, nephric genes started to be expressed, and in the final step, the expressions of *Pax2*, *Six2*, *Gdnf*, and posterior *Hox* genes increased to the levels in the embryonic MM. We further confirmed the colocalization of multiple transcription factors in single cells, such as Wt1/Pax2 and Sall1/Six2 (Figure 4I), and the existence of the Itga8$^+$/Pdgfra$^-$ population (30.8% ± 2.4%, n = 4) in the induced spheres (Figure 4J). Taken together, we established a protocol to induce metanephric nephron progenitors from the posterior nascent mesoderm.

Metanephric Nephron Progenitor Induction from Mouse ESCs

Next, we tried to induce metanephric nephron progenitors from ESCs. To monitor the induction of intermediate mesoderm and metanephric nephron progenitors, we employed the *Osr1-GFP* ESC line, from which we generated the *Osr1-GFP* mice described above. Embryoid bodies (EBs) were generated in serum-free medium without any factors for 2 days (Gadue et al., 2006) (Figure 5A). During the following 24 hr, a low concentration of activin induced transient expression of the epiblast marker *Fgf5* (Figure 5B). The EBs were subsequently treated with Bmp4 and a high concentration of Wnt agonist (10 μM CHIR). At day 4.5, the expressions of *T*, as well as *Cdx2* and *Tbx6*, which represent the posterior nascent mesoderm, were upregulated. Subsequently, we completely mimicked the protocol for the embryonic posterior mesoderm (Figures 4C and 5A; steps 3–5). The induced EBs harvested at day 8.5 expressed multiple signature genes for metanephric nephron progenitors at comparable levels to the embryonic MM (Figure 5B). Immunostaining showed that many cells coexpressed typical metanephric nephron progenitor markers, including Osr1, Wt1, Pax2, Sall1, and Six2 (Figure 5C). Furthermore, FACS analyses showed that nearly 90% of the cells were Osr1-GFP$^+$, and among the Osr1$^+$ cells, Itga8$^+$/Pdgfra$^-$ progenitors constituted approximately 65% (Figure 5D). These induced progenitors exhibited robust colony formation (21.3% ± 1.7%, n = 8). Therefore, we succeeded in generating metanephric nephron progenitors from mouse ESCs. It is of note that the in vivo MM in the E11.5 embryo contains another cell type, stromal cells, located in the outer layer of the nephron progenitors (Humphreys et al., 2010; Mugford et al., 2008b). As shown in Figures 1E and 1G, these stromal cells were included in the Osr1$^+$/Pdgfra$^+$/Itga8^{low} population. Although our induced EBs contained some Pdgfra$^+$ cells (Figure 5D), the expressions of stromal cell marker genes, including *Foxd1*, *Rarb*, and *Pbx1* (Hatini et al., 1996; Mendelsohn et al., 1999; Schnabel et al., 2003), were comparable to those in the E11.5 embryonic Six2$^+$ nephron progenitors and much lower than those in the stroma of the kidney (Figure 5E). Therefore, our protocol directs the cells specifically toward the nephron progenitors, but not the stroma.

3D Kidney Structures Formed by ESCs

It is well established that the MM from E11.5 embryos undergoes mesenchymal-to-epithelial transition and forms glomeruli and renal tubules when cocultured with embryonic spinal cords or Wnt4-expressing cells at the air-liquid interface (Kispert et al., 1998) (Figures 6A and 6B). Therefore, we cultured the induced EBs in the same manner, which resulted in robust tubulogenesis. Specifically, histological examination of EBs harvested at day 6 identified many tubules under both conditions (Figures 6C, 6D, and S6A). Most of the tubules were positive for Pax2 and Sall1, indicating that they were renal tubules (Figures 6E–6H). Some tubules expressed markers for proximal tubules, such as LTL, Cadherin6, Aquaporin1, Jagged1, and Megalin (Figures 6F, 6G, and 6L–6N). Other tubules showed expressions of E-cadherin, Brn1, and NCC, indicative of distal tubule formation (Figures 6H, 6O, and 6P). More impressively, numerous glomerulus-like structures were observed (Figures 6D and 6I). These structures contained clusters of cells that expressed a typical podocyte marker, Wt1, in their nuclei, as well as foot process proteins such as nephrin and podocin (Figures 6I–6K). These structures were indistinguishable from those of the embryonic MM (Figures 6A and 6B, n = 6). On the other hand, the EBs cultured without factors after step 2 (Figure 5A) showed some neural rosette-like formations, but no kidney tubule or glomeruli formations (Figure S6B).

Figure 4. Metanephric Nephron Progenitor Induction from the E8.5 T$^+$ Posterior Nascent Mesoderm

(A) T-GFP expression in the E8.5 embryo is shown. Bright field (left panel) and the fluorescence (right panel) are presented. Scale bar, 500 μm. The presomitic mesoderm region is outlined by the dashed line.

(B) The gate for T-GFP$^+$ cell population sorting is shown.

(C and D) Culture conditions are shown for (E)–(G). A, Activin; B, Bmp4; C, CHIR; R, retinoic acid; F, Fgf9.

(E and F) Relative expression of each transcript to β-actin expression is presented as the mean ± SEM (n = 4). E10.5MM, E10.5 Metanephric Mesenchyme; T-GFP$^+$, starting sample.

(G) Colony-forming ratios of cultured cell aggregates are presented. Data are shown as the mean ± SEM (n = 4).

(H) Temporal kinetics of marker genes is shown. The expression levels in the E10.5 embryonic MM are shown in red. The relative expression of each transcript to β-actin expression is presented as the mean ± SEM (n = 4).

(I) Immunostaining of induced cell aggregates is presented. High-magnification images are shown in the right two panels. Scale bars, 200 μm (left six panels) and 20 μm (right two panels).

(J) FACS analysis of Itga8/Pdgfra expression at day 4 is shown.

See also Figures S4 and S5.

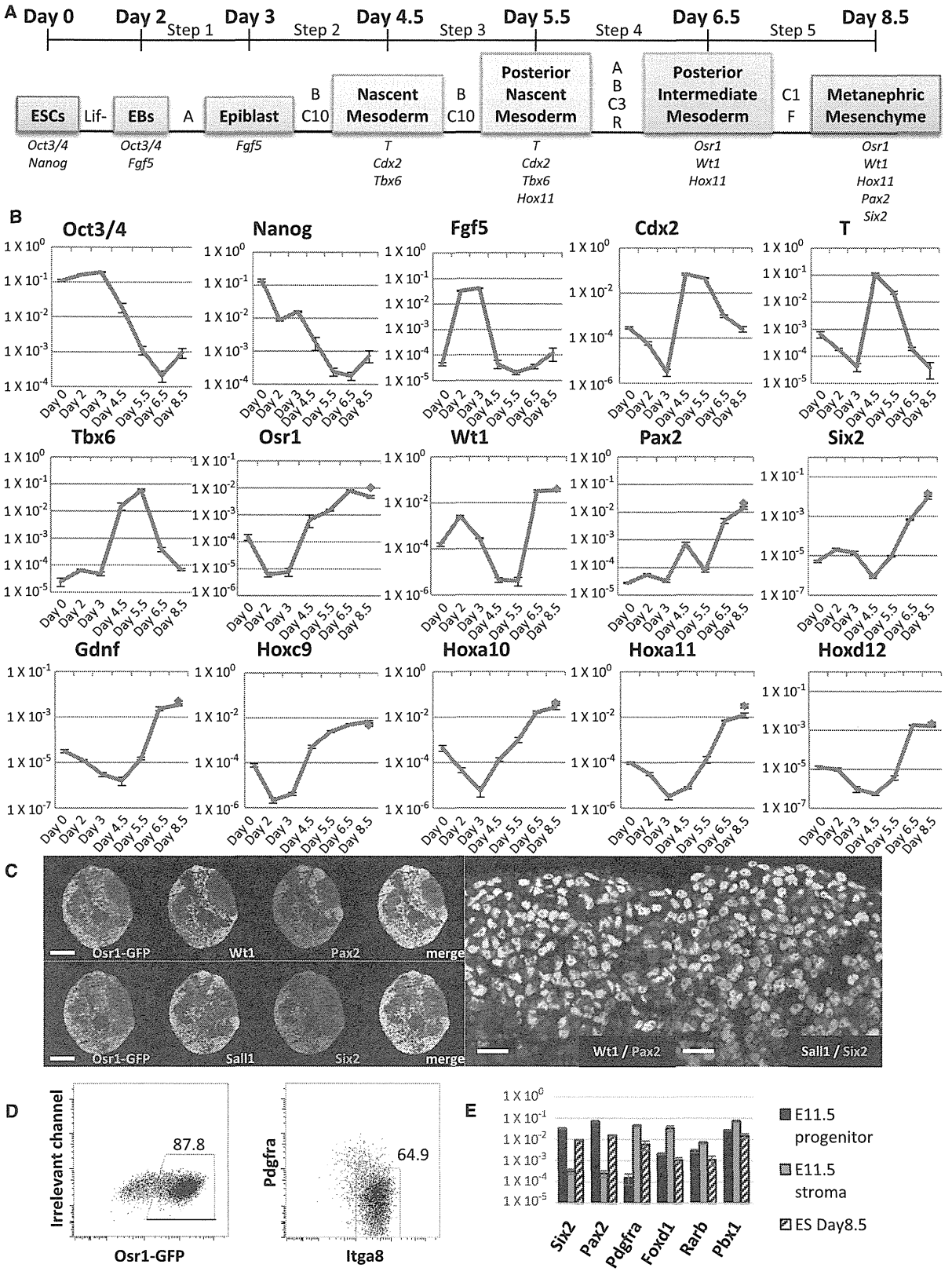

(legend on next page)

We further used another ESC line with ubiquitous expression of dsRed and transplanted the induced EBs beneath the kidney capsule of immunodeficient mice, together with spinal cords (Figures 6Q, 6R, S6C, and S6D). When harvested after 1 week, the rudiments had undergone massive tubulogenesis, similar to the in vitro cultures (Figures 6R–6T). Furthermore, many blood vessels had integrated into the transplanted tissue, including ESC-derived glomeruli (Figures 6U–6W, 22 of 26 glomeruli [84.6%]). Notably, the glomerular podocytes in the graft tissue expressed vascular growth factors, including Vegfa and Ephrin B2, both of which are indispensable for endothelial capillary formation in the glomeruli (Figures 6X and 6Y) (Eremina et al., 2003; Takahashi et al., 2001). Importantly, the vascularized glomeruli contained red blood cells (Figure 6U), and the integrated vessels were negative for dsRed (Figure S6E), indicating that the transplanted glomeruli could become connected to the host circulation, which is an essential requirement for the glomerular function as a filtration apparatus.

Metanephric Nephron Progenitor Induction from Human iPSCs

We further applied our protocol to human iPSC differentiation toward metanephric nephron progenitors in vitro. Previous reports showed the importance of Bmp, Fgf, and activin signals for the initial induction of mesodermal lineage cells for human PSCs (Bernardo et al., 2011; Kattman et al., 2011). Therefore, we treated human iPSC aggregates with Bmp for the initial 24 hr, followed by activin and Fgf for the next 2 days. The induced mesodermal cells were further posteriorized and maintained in the immature mesoderm state in the presence of a high concentration of Wnt agonist (CHIR 10 μM) and Bmp, similar to mouse ESC induction. Given the physiological time period for caudal body extension in human embryos, we cultured EBs under these culture conditions for 6 days. Subsequently, we completely mimicked the protocol for mouse ESC differentiation by simply adjusting the culture periods (Figure 7A). The induced EBs harvested at day 14 expressed multiple signature genes for metanephric nephron progenitors (Figure 7B). Immunostaining revealed that many cells coexpressed typical nephrogenic transcription factors, including Wt1, Pax2, Sall1, and Six2 (Figure 7C). The induced EBs were further dissociated, and the induction efficiency was quantified by cytospin analyses. When the EBs were collected at day 11 (posterior intermediate mesoderm phase), more than 80% of the cells were positive for Wt1 (Figure S7A, n = 9). Analysis at day 14 (MM stage) showed that 20%–70% of the cells were positive for each representative metanephric nephron progenitor marker, including Wt1, Pax2, Sall1, and Six2 (Figure S7B, n = 9). Furthermore, these induced progenitors exhibited robust tubulogenesis and clustered podocyte formation when cocultured with mouse embryonic spinal cords (Figures 7D and 7E, n = 6). Immunohistochemical examinations at day 8 revealed the formation of well-specified nephron components. These structures consisted of Wt1/nephrin$^+$ glomeruli (Figures 7F and 7G), cadherin6$^+$ proximal tubules (Figure 7H), and E-cadherin$^+$ distal tubules (Figure 7I), all of which appeared to be connected in that order, thereby mimicking human embryonic kidney formation. In conclusion, we succeeded in the induction of bona fide metanephric nephron progenitors and three-dimensional (3D) kidney structures from both mouse and human PSCs, by recapitulating the developmental processes in vivo (Figure 7J).

DISCUSSION

We have succeeded in inducing metanephric nephron progenitors capable of reconstituting 3D nephric tubules and glomeruli, the two main components that are critical for kidney functions, from mouse and human PSCs. These findings will be useful for revealing molecular mechanisms underlying human kidney diseases and open a way for regenerative medicine in the future. Our data also demonstrate that the developmental processes of the kidney are well conserved between humans and mice, and emphasize the robustness of our protocol that faithfully mimics the physiological processes. Our success relies on the approach that we initially determined the conditions for the later phase (from E9.5 to 10.5) and then progressed toward the earlier phases (from E8.5 to 10.5, and then ES to E10.5) by using embryonic tissue instead of starting from ESCs. The induction of kidney progenitors requires multiple steps, but reliable markers and detection assays were only available for the MM stage. Therefore, we could not have verified whether the induced ESCs in the early steps possessed the capacity to differentiate into nephron progenitors, unless all of the subsequent conditions had been optimized. Consequently, a conventional forward approach would not have been helpful. Our backward approach using fully "competent" embryonic precursors proved to be very effective and could be applicable to other organ induction.

Brachyury (*T*), which starts to be expressed at the gastrulation stage, has been recognized as a "transient" mesodermal marker in studies of directed differentiation from stem cells. However, it has recently been shown that the immature caudal population, namely the "axial progenitor," persists in the posterior end of the embryo until the body axis extension is complete, and serves as the source of the caudal body trunk (Takemoto et al., 2011; Tzouanacou et al., 2009; Wilson et al., 2009). Our data suggest that this recently identified posterior precursor population could

Figure 5. Metanephric Nephron Progenitor Induction from Mouse ESCs

(A) Outline of the protocol is presented. A, activin; B, Bmp4; C, CHIR; R, retinoic acid; F, Fgf9.

(B) *Gene expression dynamics during the induction from ESCs is presented. The expression levels in the E10.5 embryonic MM are shown in red.* The relative expression of each transcript to β-actin expression is presented as the mean ± SEM (n = 4).

(C) Localizations of Osr1-GFP/Wt1/Pax2$^+$ and Osr1-GFP/Sall1/Six2$^+$ cells in the induced EBs at day 8.5 are presented. The right two panels show higher-magnification images. Scale bars, 200 μm (left eight panels) and 20 μm (right two panels).

(D) FACS analyses of Osr1-GFP and Itga8/Pdgfra expressions in EBs at day 8.5 are shown.

(E) Gene expression analyses of the E11.5 Six2$^+$ embryonic nephron progenitor and stromal populations (Osr1$^+$/Itga$^+$/Pdgfra$^-$ and Osr1$^+$/Itga^{low}/Pdgfra$^+$, respectively, sorted by FACS) and day 8.5 differentiated ESCs are shown. The relative expression of each transcript to β-actin expression is presented as the mean ± SEM (n = 3).

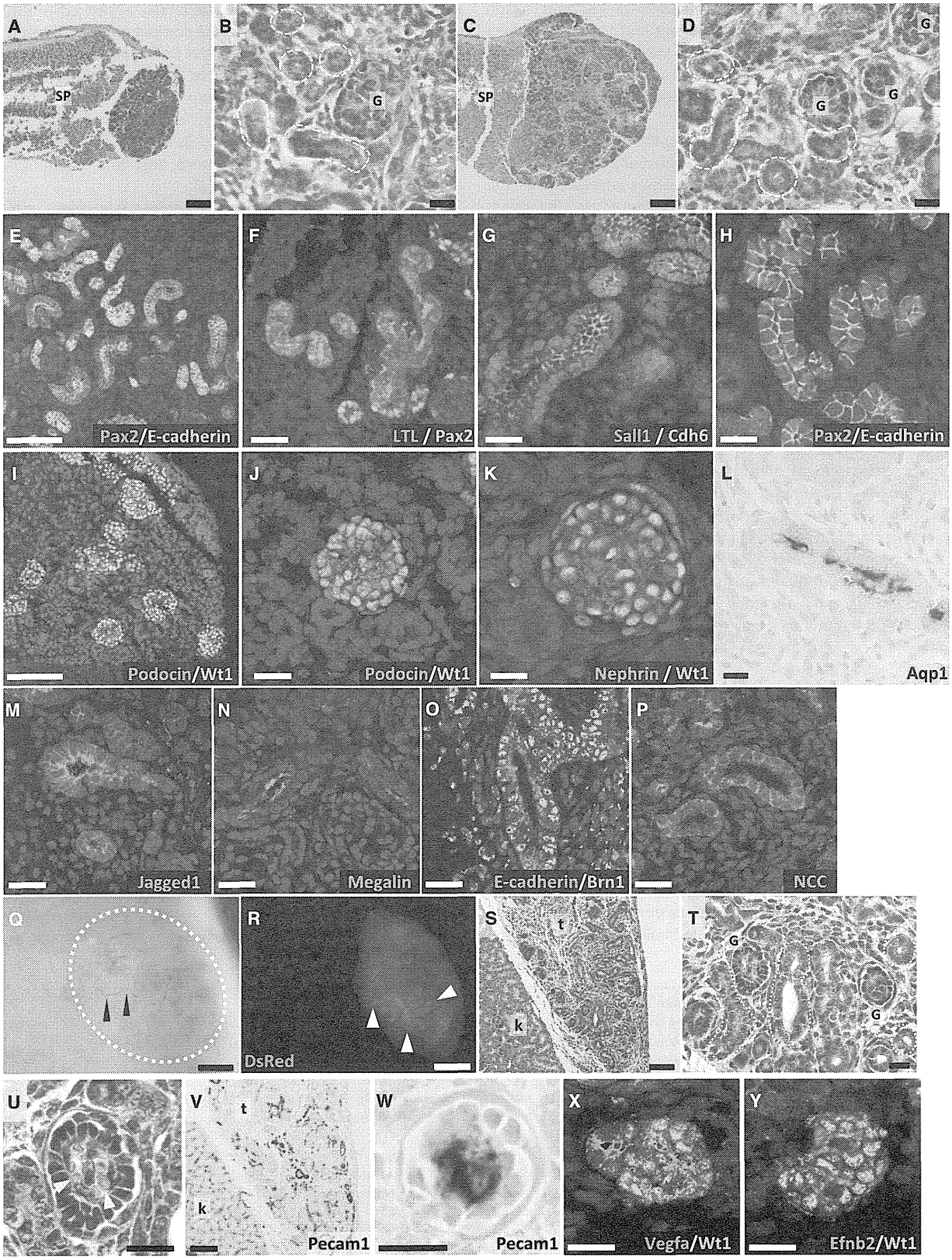

(legend on next page)

also be the origin of the MM, i.e., nephron progenitors, which argues against the conventional concept that the entire kidney is derived from the anteriorly formed intermediate mesoderm that extends caudally. The introduction of this axial progenitor model may be further applied for directed differentiation toward other caudally located organs.

In vitro, we succeeded in maintaining the T^+ state during the posteriorization phase by utilizing an unusually high concentration of Wnt agonist. Subsequently, graded attenuation of the Wnt agonist, as well as stage-specific addition of growth factors, allowed nephric lineage commitment and metanephric nephron progenitor formation. The necessity for high concentrations of the Wnt agonist in the initial phase of the induction could reflect the importance of Wnt signaling for the caudal body extension and maintenance of axial progenitors (Wilson et al., 2009; Yamaguchi et al., 1999). In the following step toward the posterior intermediate mesoderm, decreasing the Wnt agonist concentration and addition of retinoic acid are effective, similar to the caudal differentiation process of the paraxial mesoderm (Aulehla and Pourquié, 2010). The synergistic effect of activin on the nephric gene induction is reminiscent of a previous finding that a combination of activin and retinoic acid induces the pronephros-like structures in *Xenopus* animal caps (Moriya et al., 1993). Subsequently, addition of Fgf9 and a further reduction in Wnt signaling lead to the appearance of the metanephric nephron progenitors, and exogenous Bmp4, retinoic acid, and activin should be removed at this final step, indicating stage-specific requirements for each type of signaling (Figure 7J). These observations may partly explain why we failed to induce metanephric progenitors from $Osr1^+$ cells at E8.5. It is possible that $Osr1^+$ cells already present at E8.5 do not contribute to the metanephros and that the $T^+/Osr1^-$ population gives rise to genuine $T^-/Osr1^+$ cells that are competent for metanephros differentiation. The $Osr1^+$ cells that emerge during E8.5–E9.5 may have become labeled and contributed to the metanephros in a previously reported lineage-tracing study by Mugford et al. (2008b), although more detailed analyses are needed to test this possibility.

The nephron progenitors obtained from embryos readily form the 3D glomeruli and renal tubules when combined with spinal cord or upon Wnt stimulation. This should hold true for the progenitors induced in vitro, and our cells completely meet these criteria. Although a few studies have challenged the induction of kidney progenitors (Mae et al., 2013; Narayanan et al., 2013), they lacked the ideas that the competence of intermediate mesoderm is temporally (E8.5 versus E9.5) and spatially (anteroposteriorly) different and considered $Osr1^+$or $Pax2^+$ cells to be a homogeneous population. This could result in failure of the formation of 3D glomeruli, an essential feature of the metanephros. Thus, the capacity of the induced cells in the other reports would be quite different from that of our cells, despite the Osr1 or Pax2 expression.

Although we still need to further mature the nephron components, and also combine them with ureteric bud-derived structures to confer the physiological functions of the kidney, our study will be a big step toward kidney reconstruction in vitro. Combinations of developmental biology and stem cell biology, as shown in this report, will be effective to achieve this goal.

EXPERIMENTAL PROCEDURES

Sorted Embryonic Cell Culture

For embryonic tissue cultures at E8.5, the presomitic regions of six to ten somite-stage embryos were harvested, and T-GFP^+ cells were sorted by a FACSAria II (Becton Dickinson). The sorted cells were aggregated at 7,000 cells per aggregate in 96-well low-cell-binding plates and cultured in serum-free chemically defined medium. In the embryonic tissue cultures at E9.5, the posterior regions from the 23rd somite region of 22–26 somite-stage embryos were harvested, and Osr1-GFP^+ or Wt1-GFP^+ cells were sorted. The sorted cells were aggregated at 10,000 cells per aggregate and cultured. All animal experiments were approved by the Animal Care and Use Committee of Kumamoto University (#A25-062).

Mouse ESC and Human iPSC Culture

Mouse ESCs were aggregated at 1,000 cells per aggregate in 96-well U-bottom low-cell-binding plates to form EBs. After 48 hr (on day 2), the EBs were dissociated with Accutase and reaggregated in serum-free differentiation medium with addition of 0.5 or 1 ng/ml human activin A (R&D Systems). After 24 hr, the medium was switched to BC10 medium containing 1 ng/ml human Bmp4 (R&D Systems) and 10 μM CHIR. After 36 hr, (on day 4.5), the medium was refreshed with new medium (BC10). On day 5.5, the medium was changed to ABC3R medium containing 10 ng/ml activin, 3 ng/ml Bmp4, 3 μM CHIR, 0.1 μM retinoic acid, and 10 μM Y27632 (Wako). On day 6.5, the medium was changed to C1F medium containing 1 μM CHIR, 5 ng/ml human Fgf9 (R&D Systems), and 10 μM Y27632 (Wako).

Human iPSCs (201B7, Takahashi et al., 2007), which were obtained from RIKEN BioResource Center, were aggregated at 10,000 cells per aggregate in V-bottom 96-well low-cell-binding plates to form EBs, in the presence of 10 μM Y27632 (Wako) and 0.5 ng/ml human Bmp4 (R&D Systems). After 24 hr (on day 1), the medium was changed to mesoderm-inducing medium

Figure 6. 3D Kidney Structures from Mouse ESCs

(A–D) Hematoxylin and eosin staining shows the embryonic MM (A and B) and induced EB (C and D) cocultured with the spinal cord (higher magnification in B and D). The nephric tubules are outlined by dashed lines. SP, spinal cord; G, glomerulus. Scale bars, 200 μm (A and C) and 20 μm (B and D).

(E–P) Immunostaining shows induced EBs for nephric tubule markers (E–H and L–P) and glomerular markers (I–K). Scale bars, 200 μm (E), 100 μm (I), and 20 μm (F–H and J–P).

(Q and R) Views present mouse kidneys excised at 1 week after being grafted with the induced EBs. The transplanted tissue is outlined by a dashed line. (Q) The black arrowheads show vascularization of the graft. (R) Fluorescence image shows the graft. The white arrowheads show nephron-like structures in the graft. Scale bars, 500 μm.

(S–U) Hematoxylin and eosin staining shows the grafted kidney sections. (S) Lower-magnification image is presented. t, transplanted tissue; k, host kidney. Scale bar, 100 μm. (T) Medium-magnification image is shown. The nephric tubules are outlined by dashed lines. G, glomerulus. Scale bar, 20 μm. (U) High-magnification image shows a glomerulus in the graft. The arrowheads indicate red blood cells in the vasculature invading the glomerulus. Scale bar, 20 μm.

(V and W) Immunostaining with blood vessel marker Pecam1 is shown. Scale bars, 20 μm.

(V) Lower-magnification image is shown. t, transplanted tissue; k, host kidney.

(W) High-magnification image shows a glomerulus in the graft.

(X and Y) Immunostaining shows glomeruli in the graft tissue for vascular growth factor markers. Scale bars, 20 μm.

See also Figure S6.

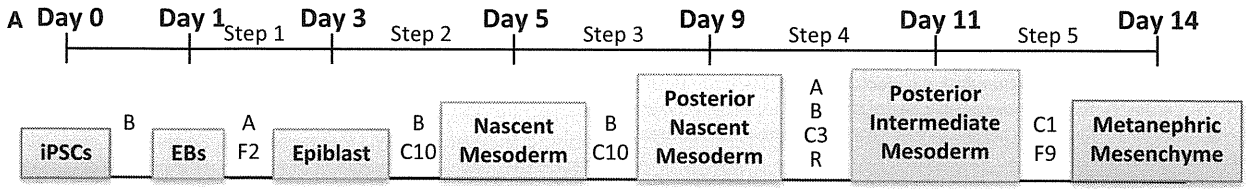

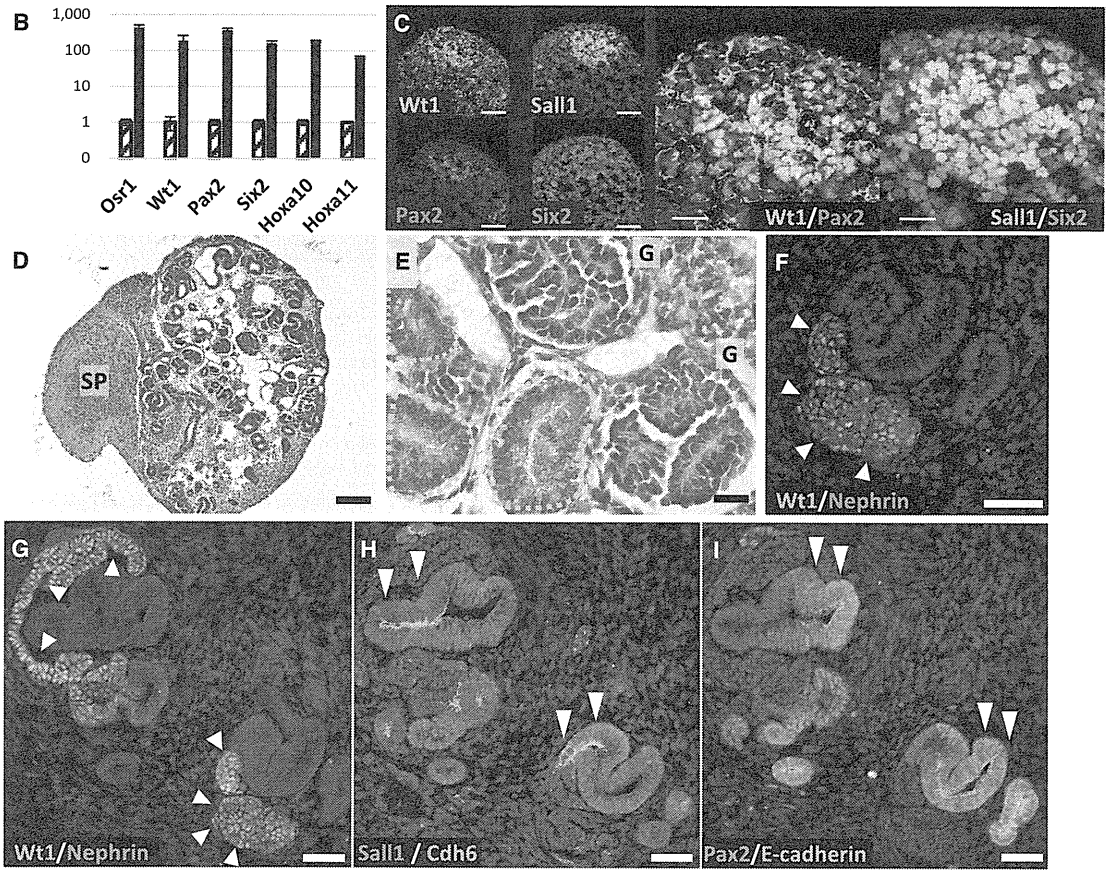

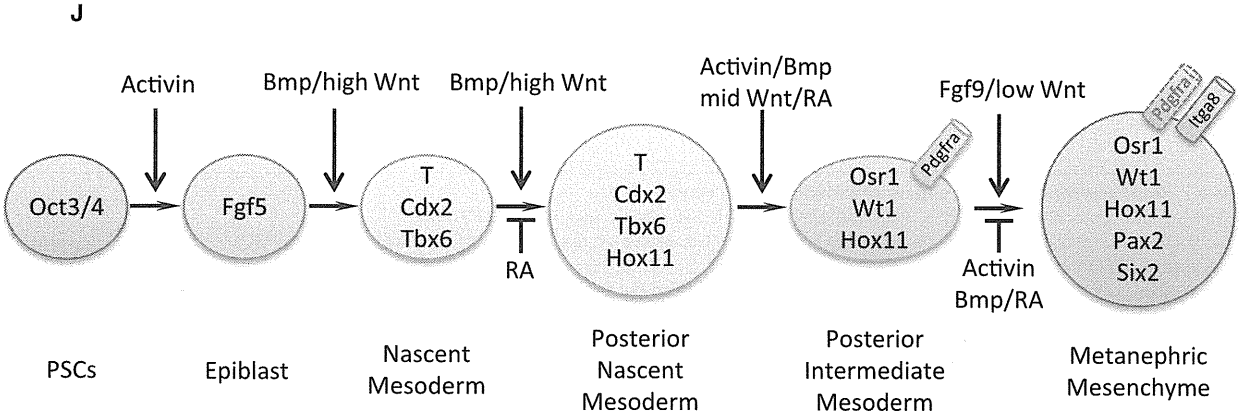

(legend on next page)

containing 1 ng/ml human activin A and 20 ng/ml human basic Fgf (R&D Systems). After 48 hr (on day 3), the medium was switched to BC10 medium. Subsequently, half of the culture medium volume was refreshed with new medium every other day (BC10). On day 9, the medium was changed to ABC3R medium. On day 11, the medium was changed to C1F medium. All data shown are representative examples of at least three independent experiments, unless indicated otherwise.

Organ Culture of MM or Induced Metanephric Progenitors

The mesenchyme rudiments or induced ESC aggregates were cultured with embryonic spinal cord taken from E11.5 or E12.5 embryos or on 3T3Wnt4 cells at the air-fluid interface on a polycarbonate filter (0.8 μm; Whatman) supplied with DMEM containing 10% fetal calf serum, as described previously by Kispert et al. (1998) and Osafune et al. (2006).

ACCESSION NUMBERS

The microarray data have been deposited in the National Center for Biotechnology Information Gene Expression Omnibus (GSE51054).

SUPPLEMENTAL INFORMATION

Supplemental Information includes Supplemental Experimental Procedures, seven figures, and two tables and can be found with this article online at http://dx.doi.org/10.1016/j.stem.2013.11.010.

ACKNOWLEDGMENTS

We thank H. Sakamoto, S.S. Tanaka, Y. Uchiyama, S. Fujimura, N. Takeda, U. Imuta, D. Toyoda, D. Sakano, and K. Suzuki for technical advice and assistance; G. Dressler and K. Asanuma for providing the antibodies; and Y. Tomino for encouragement. This work was supported in part by KAKENHI Grants (21116003, 23390228, and 32534020) from the Ministry of Education, Culture, Sports, Science and Technology (MEXT), Japan Society for the Promotion of Science, and the Ministry of Health, Labor and Welfare, the Global COE Program (Cell Fate Regulation Research and Education Unit, MEXT), and the Japan Science and Technology Agency, CREST.

Received: July 11, 2013
Revised: September 20, 2013
Accepted: November 12, 2013
Published: December 12, 2013

REFERENCES

Atsuta, Y., Tadokoro, R., Saito, D., and Takahashi, Y. (2013). Transgenesis of the Wolffian duct visualizes dynamic behavior of cells undergoing tubulogenesis in vivo. Dev. Growth Differ. *55*, 579–590.

Attia, L., Yelin, R., and Schultheiss, T.M. (2012). Analysis of nephric duct specification in the avian embryo. Development *139*, 4143–4151.

Aulehla, A., and Pourquié, O. (2010). Signaling gradients during paraxial mesoderm development. Cold Spring Harb. Perspect. Biol. *2*, a000869.

Barak, H., Huh, S.H., Chen, S., Jeanpierre, C., Martinovic, J., Parisot, M., Bole-Feysot, C., Nitschké, P., Salomon, R., Antignac, C., et al. (2012). FGF9 and FGF20 maintain the stemness of nephron progenitors in mice and man. Dev. Cell *22*, 1191–1207.

Bernardo, A.S., Faial, T., Gardner, L., Niakan, K.K., Ortmann, D., Senner, C.E., Callery, E.M., Trotter, M.W., Hemberger, M., Smith, J.C., et al. (2011). BRACHYURY and CDX2 mediate BMP-induced differentiation of human and mouse pluripotent stem cells into embryonic and extraembryonic lineages. Cell Stem Cell *9*, 144–155.

Bollig, F., Perner, B., Besenbeck, B., Köthe, S., Ebert, C., Taudien, S., and Englert, C. (2009). A highly conserved retinoic acid responsive element controls wt1a expression in the zebrafish pronephros. Development *136*, 2883–2892.

Bouchard, M., Souabni, A., Mandler, M., Neubüser, A., and Busslinger, M. (2002). Nephric lineage specification by Pax2 and Pax8. Genes Dev. *16*, 2958–2970.

Burridge, P.W., Keller, G., Gold, J.D., and Wu, J.C. (2012). Production of de novo cardiomyocytes: human pluripotent stem cell differentiation and direct reprogramming. Cell Stem Cell *10*, 16–28.

Costantini, F., and Kopan, R. (2010). Patterning a complex organ: branching morphogenesis and nephron segmentation in kidney development. Dev. Cell *18*, 698–712.

Eremina, V., Sood, M., Haigh, J., Nagy, A., Lajoie, G., Ferrara, N., Gerber, H.P., Kikkawa, Y., Miner, J.H., and Quaggin, S.E. (2003). Glomerular-specific alterations of VEGF-A expression lead to distinct congenital and acquired renal diseases. J. Clin. Invest. *111*, 707–716.

Fleming, B.M., Yelin, R., James, R.G., and Schultheiss, T.M. (2013). A role for Vg1/Nodal signaling in specification of the intermediate mesoderm. Development *140*, 1819–1829.

Gadue, P., Huber, T.L., Paddison, P.J., and Keller, G.M. (2006). Wnt and TGF-beta signaling are required for the induction of an in vitro model of primitive streak formation using embryonic stem cells. Proc. Natl. Acad. Sci. USA *103*, 16806–16811.

Hatini, V., Huh, S.O., Herzlinger, D., Soares, V.C., and Lai, E. (1996). Essential role of stromal mesenchyme in kidney morphogenesis revealed by targeted disruption of Winged Helix transcription factor BF-2. Genes Dev. *10*, 1467–1478.

Herrmann, B.G., Labeit, S., Poustka, A., King, T.R., and Lehrach, H. (1990). Cloning of the T gene required in mesoderm formation in the mouse. Nature *343*, 617–622.

Humphreys, B.D., Lin, S.L., Kobayashi, A., Hudson, T.E., Nowlin, B.T., Bonventre, J.V., Valerius, M.T., McMahon, A.P., and Duffield, J.S. (2010). Fate tracing reveals the pericyte and not epithelial origin of myofibroblasts in kidney fibrosis. Am. J. Pathol. *176*, 85–97.

Imuta, Y., Kiyonari, H., Jang, C.W., Behringer, R.R., and Sasaki, H. (2013). Generation of knock-in mice that express nuclear enhanced green fluorescent protein and tamoxifen-inducible Cre recombinase in the notochord from Foxa2 and T loci. Genesis *51*, 210–218.

James, R.G., Kamei, C.N., Wang, Q., Jiang, R., and Schultheiss, T.M. (2006). Odd-skipped related 1 is required for development of the metanephric

Figure 7. Metanephric Nephron Progenitor Induction from Human iPSCs

(A) Outline of the protocol is presented. A, Activin; B, Bmp4; C, CHIR; R, retinoic acid; F2, Fgf2; F9, Fgf9.

(B) Gene expression analyses of the differentiated iPSCs are shown. The relative expression of each transcript to immature iPSCs (each left column) is presented as the mean ± SEM (n = 6).

(C) Localizations of Wt1/Pax2$^+$ and Sall1/Six2$^+$ cells in the induced EBs at day 14 are shown. The right two panels show higher-magnification images. Scale bars, 75 μm (left four panels) and 20 μm (right two panels).

(D and E) Hematoxylin and eosin staining shows the induced EBs cocultured with spinal cord (D) and a higher-magnification image (E). The nephric tubules are outlined by dashed lines. SP, spinal cord; G, glomerulus. Scale bars, 200 μm (D) and 20 μm (E).

(F–I) Immunostaining shows neighboring sections of induced EBs for glomerular markers (F and G) and nephric tubule markers (H and I). Arrowheads indicate the glomeruli in (F and G), the proximal tubule segments in (H), and the distal tubule segments in (I). Scale bars, 50 μm.

(J) Model of directed differentiation of PSCs toward the MM is presented.

See also Figure S7.

kidney and regulates formation and differentiation of kidney precursor cells. Development *133*, 2995–3004.

Kattman, S.J., Witty, A.D., Gagliardi, M., Dubois, N.C., Niapour, M., Hotta, A., Ellis, J., and Keller, G. (2011). Stage-specific optimization of activin/nodal and BMP signaling promotes cardiac differentiation of mouse and human pluripotent stem cell lines. Cell Stem Cell *8*, 228–240.

Kim, D., and Dressler, G.R. (2005). Nephrogenic factors promote differentiation of mouse embryonic stem cells into renal epithelia. J. Am. Soc. Nephrol. *16*, 3527–3534.

Kispert, A., Vainio, S., and McMahon, A.P. (1998). Wnt-4 is a mesenchymal signal for epithelial transformation of metanephric mesenchyme in the developing kidney. Development *125*, 4225–4234.

Kobayashi, A., Valerius, M.T., Mugford, J.W., Carroll, T.J., Self, M., Oliver, G., and McMahon, A.P. (2008). Six2 defines and regulates a multipotent self-renewing nephron progenitor population throughout mammalian kidney development. Cell Stem Cell *3*, 169–181.

Lengerke, C., Schmitt, S., Bowman, T.V., Jang, I.H., Maouche-Chretien, L., McKinney-Freeman, S., Davidson, A.J., Hammerschmidt, M., Rentzsch, F., Green, J.B., et al. (2008). BMP and Wnt specify hematopoietic fate by activation of the Cdx-Hox pathway. Cell Stem Cell *2*, 72–82.

Li, X., Pontén, A., Aase, K., Karlsson, L., Abramsson, A., Uutela, M., Bäckström, G., Hellström, M., Boström, H., Li, H., et al. (2000). PDGF-C is a new protease-activated ligand for the PDGF alpha-receptor. Nat. Cell Biol. *2*, 302–309.

Madisen, L., Zwingman, T.A., Sunkin, S.M., Oh, S.W., Zariwala, H.A., Gu, H., Ng, L.L., Palmiter, R.D., Hawrylycz, M.J., Jones, A.R., et al. (2010). A robust and high-throughput Cre reporting and characterization system for the whole mouse brain. Nat. Neurosci. *13*, 133–140.

Mae, S., Shono, A., Shiota, F., Yasuno, T., Kajiwara, M., Gotoda-Nishimura, N., Arai, S., Sato-Otubo, A., Toyoda, T., Takahashi, K., et al. (2013). Monitoring and robust induction of nephrogenic intermediate mesoderm from human pluripotent stem cells. Nat. Commun. *4*, 1367.

Mendelsohn, C., Batourina, E., Fung, S., Gilbert, T., and Dodd, J. (1999). Stromal cells mediate retinoid-dependent functions essential for renal development. Development *126*, 1139–1148.

Moriya, N., Uchiyama, H., and Asashima, M. (1993). Induction of pronephric tubules by activin and retinoic acid in presumptive ectoderm of *Xenopus laevis*. Dev. Growth Differ. *35*, 123–128.

Mugford, J.W., Sipilä, P., Kobayashi, A., Behringer, R.R., and McMahon, A.P. (2008a). Hoxd11 specifies a program of metanephric kidney development within the intermediate mesoderm of the mouse embryo. Dev. Biol. *319*, 396–405.

Mugford, J.W., Sipilä, P., McMahon, J.A., and McMahon, A.P. (2008b). Osr1 expression demarcates a multi-potent population of intermediate mesoderm that undergoes progressive restriction to an Osr1-dependent nephron progenitor compartment within the mammalian kidney. Dev. Biol. *324*, 88–98.

Müller, U., Wang, D., Denda, S., Meneses, J.J., Pedersen, R.A., and Reichardt, L.F. (1997). Integrin alpha8beta1 is critically important for epithelial-mesenchymal interactions during kidney morphogenesis. Cell *88*, 603–613.

Murry, C.E., and Keller, G. (2008). Differentiation of embryonic stem cells to clinically relevant populations: lessons from embryonic development. Cell *132*, 661–680.

Narayanan, K., Schumacher, K.M., Tasnim, F., Kandasamy, K., Schumacher, A., Ni, M., Gao, S., Gopalan, B., Zink, D., and Ying, J.Y. (2013). Human embryonic stem cells differentiate into functional renal proximal tubular-like cells. Kidney Int. *83*, 593–603.

Nelson, L.T., Rakshit, S., Sun, H., and Wellik, D.M. (2008). Generation and expression of a Hoxa11eGFP targeted allele in mice. Dev. Dyn. *237*, 3410–3416.

Nishinakamura, R., Matsumoto, Y., Nakao, K., Nakamura, K., Sato, A., Copeland, N.G., Gilbert, D.J., Jenkins, N.A., Scully, S., Lacey, D.L., et al. (2001). Murine homolog of SALL1 is essential for ureteric bud invasion in kidney development. Development *128*, 3105–3115.

Obara-Ishihara, T., Kuhlman, J., Niswander, L., and Herzlinger, D. (1999). The surface ectoderm is essential for nephric duct formation in intermediate mesoderm. Development *126*, 1103–1108.

Osafune, K., Takasato, M., Kispert, A., Asashima, M., and Nishinakamura, R. (2006). Identification of multipotent progenitors in the embryonic mouse kidney by a novel colony-forming assay. Development *133*, 151–161.

Poladia, D.P., Kish, K., Kutay, B., Hains, D., Kegg, H., Zhao, H., and Bates, C.M. (2006). Role of fibroblast growth factor receptors 1 and 2 in the metanephric mesenchyme. Dev. Biol. *291*, 325–339.

Saxen, L. (1987). Organogenesis of the Kidney. (New York: Cambridge University Press).

Schnabel, C.A., Godin, R.E., and Cleary, M.L. (2003). Pbx1 regulates nephrogenesis and ureteric branching in the developing kidney. Dev. Biol. *254*, 262–276.

Takahashi, K., Tanabe, K., Ohnuki, M., Narita, M., Ichisaka, T., Tomoda, K., and Yamanaka, S. (2007). Induction of pluripotent stem cells from adult human fibroblasts by defined factors. Cell *131*, 861–872.

Takahashi, T., Takahashi, K., Gerety, S., Wang, H., Anderson, D.J., and Daniel, T.O. (2001). Temporally compartmentalized expression of ephrin-B2 during renal glomerular development. J. Am. Soc. Nephrol. *12*, 2673–2682.

Takemoto, T., Uchikawa, M., Yoshida, M., Bell, D.M., Lovell-Badge, R., Papaioannou, V.E., and Kondoh, H. (2011). Tbx6-dependent Sox2 regulation determines neural or mesodermal fate in axial stem cells. Nature *470*, 394–398.

Tam, P.P., and Behringer, R.R. (1997). Mouse gastrulation: the formation of a mammalian body plan. Mech. Dev. *68*, 3–25.

Tzouanacou, E., Wegener, A., Wymeersch, F.J., Wilson, V., and Nicolas, J.-F. (2009). Redefining the progression of lineage segregations during mammalian embryogenesis by clonal analysis. Dev. Cell *17*, 365–376.

Watanabe, K., Ueno, M., Kamiya, D., Nishiyama, A., Matsumura, M., Wataya, T., Takahashi, J.B., Nishikawa, S., Nishikawa, S., Muguruma, K., and Sasai, Y. (2007). A ROCK inhibitor permits survival of dissociated human embryonic stem cells. Nat. Biotechnol. *25*, 681–686.

Wellik, D.M., Hawkes, P.J., and Capecchi, M.R. (2002). Hox11 paralogous genes are essential for metanephric kidney induction. Genes Dev. *16*, 1423–1432.

Williams, L.A., Davis-Dusenbery, B.N., and Eggan, K.C. (2012). SnapShot: directed differentiation of pluripotent stem cells. Cell *149*, 1174–1174.e1.

Wilson, V., Olivera-Martinez, I., and Storey, K.G. (2009). Stem cells, signals and vertebrate body axis extension. Development *136*, 1591–1604.

Yamaguchi, T.P., Takada, S., Yoshikawa, Y., Wu, N., and McMahon, A.P. (1999). T (Brachyury) is a direct target of Wnt3a during paraxial mesoderm specification. Genes Dev. *13*, 3185–3190.

Zhou, B., Ma, Q., Rajagopal, S., Wu, S.M., Domian, I., Rivera-Feliciano, J., Jiang, D., von Gise, A., Ikeda, S., Chien, K.R., and Pu, W.T. (2008). Epicardial progenitors contribute to the cardiomyocyte lineage in the developing heart. Nature *454*, 109–113.

Molecular Genetics and Metabolism Reports 1 (2014) 19–30

Contents lists available at ScienceDirect

Molecular Genetics and Metabolism Reports

journal homepage: http://www.journals.elsevier.com/molecular-genetics-and-metabolism-reports/

Influence of *Npc1* genotype on the toxicity of hydroxypropyl-β-cyclodextrin, a potentially therapeutic agent, in Niemann–Pick Type C disease models ☆

Yuta Tanaka [a,1], Yoichi Ishitsuka [a,1], Yusei Yamada [a], Yuki Kondo [a], Toru Takeo [b], Naomi Nakagata [b], Taishi Higashi [c], Keiichi Motoyama [c], Hidetoshi Arima [c], Muneaki Matsuo [d], Katsumi Higaki [e], Kousaku Ohno [f], Tetsumi Irie [a,*]

[a] *Department of Clinical Chemistry and Informatics, Graduate School of Pharmaceutical Sciences, Kumamoto University, 5–1 Oe-honmachi, Chuo-ku, Kumamoto 862–0973, Japan*
[b] *Division of Reproductive Engineering, Center for Animal Resources and Development (CARD), Kumamoto University, 2-2-1 Honjo Kumamoto 860–0811, Japan*
[c] *Department of Physical Pharmaceutics, Graduate School of Pharmaceutical Sciences, Kumamoto University, 5–1 Oe-honmachi, Chuo-ku, Kumamoto 862–0973, Japan*
[d] *Department of Pediatrics, Faculty of Medicine, Saga University, 5-1-1, Nabeshima, Saga, 849–8501, Saga, Japan*
[e] *Division of Functional Genomics, Research Center for Bioscience and Technology, Faculty of Medicine, Tottori University, 86 Nishi-cho, Yonago 683–8503, Japan*
[f] *Department of Child Neurology, Institute of Neurological Sciences, Faculty of Medicine, Tottori University, 36–1, Nishi-cho, Yonago, 683–8504, Japan*

ARTICLE INFO

Article history:
Received 16 December 2013
Accepted 16 December 2013
Available online xxxx

Keywords:
Niemann–Pick Type C
Hydroxypropyl-β-cyclodextrin
Npc1-deficient mice
Lysosomal storage disease
Autosomal recessive disorder
U18666A

ABSTRACT

Hydroxypropyl-β-cyclodextrin (HPBCD) is an attractive drug candidate against Niemann–Pick Type C (NPC) disease. However, the safety of HPBCD treatment for NPC patients remains to be elucidated. In this study, we examined the acute toxicity of HPBCD in *Npc1*-deficient mice. When treated with HPBCD (20,000 mg/kg, subcutaneously), over half of the wild-type ($Npc1^{+/+}$) or $Npc1^{+/-}$ mice died by 72 h after the injection. In contrast, all of the $Npc1^{-/-}$ mice survived. Marked pathophysiological changes, such as an elevation in serum transaminase and creatinine levels, hepatocellular necrosis, renal tubular damage, interstitial thickening, and hemorrhages in lungs, were induced by the HPBCD treatment in $Npc1^{+/+}$ or $Npc1^{+/-}$ mice. However, these

Abbreviations: NPC, Niemann–Pick Type C disease; HPBCD, Hydroxypropyl-β-cyclodextrin; ALT, Alanine aminotransferase; CHO, Chinese hamster ovary.

* Corresponding author. Tel./fax: +81 96 371 4552.
E-mail address: tirie@gpo.kumamoto-u.ac.jp (T. Irie).

[1] These authors contributed equally to this work.

2214-4269/$ – see front matter
http://dx.doi.org/10.1016/j.ymgmr.2013.12.003

pathophysiological changes were significantly alleviated in *Npc1*$^{-/-}$ mice. In addition, *in vitro* analysis showed that the *Npc1* gene deficiency and treatment with U18666A, an Npc1 inhibitor, remarkably attenuated the cytotoxicity of HPBCD in Chinese hamster ovary cells. These results suggest that the *NPC1* genotype exacerbates the cytotoxicity of HPBCD and *Npc1*$^{-/-}$ mice have substantial resistance to the lethality and the organ injury induced by HPBCD injection compared with *Npc1*$^{+/+}$ or *Npc1*$^{+/-}$ mice. We suggest that the *Npc1* genotype should be considered in the safety evaluation of HPBCD using experimental animals and cells.

1. Introduction

Niemann–Pick Type C (NPC) disease, an autosomal recessive disorder caused by mutations in either of the *Npc1* or *Npc2* genes, is characterized by progressive neurological deterioration and death during childhood [1]. Marked lysosomal accumulation of unesterified cholesterol and shortage of esterified cholesterol in cellular compartments are observed in NPC disease, and cholesterol sequestration may be a key factor in developing the disease. Recently, some reports have shown that hydroxypropyl-β-cyclodextrin (HPBCD), a cyclic oligosaccharide derivative that has a solubilizing ability on lipophilic compounds, including cholesterol, attenuated cholesterol sequestration in systemic cells and prolonged the lifespan in *Npc1* null mice [2–4]. In addition, Matsuo et al. [5] reported that treatment with HPBCD improved hepatosplenomegaly and central nervous system dysfunction in two patients with NPC disease.

HPBCD has been used as a pharmaceutical additive with high aqueous solubility and extremely low toxicity and has been used clinically with cardinal remedies in parenteral formulations [6]. Based on these facts, HPBCD is compassionately used to treat patients with NPC disease. In our previous study, patients were administered high-dose HPBCD (2000–2500 mg/kg) infusions twice or more per week without severe adverse events [5]. However, Chien et al. [7] reported that chronic HPBCD infusion induced the pneumonia in healthy pigs and suggested the risk of lung toxicity by HPBCD treatment for NPC disease. In addition, some reports have demonstrated that HPBCD caused organ injury, such as renal and liver dysfunction, in animals [8,9]. Therefore, the safety of HPBCD treatment for NPC patients remains to be elucidated.

Based on these facts, this study was conducted to evaluate the acute toxicity of HPBCD in NPC disease. We examined the toxic effects of HPBCD on mice as determined by survival rate, changes in serum biochemical parameters, and histological analysis in wild-type or homozygous and heterozygous *Npc1* mutant mice. In addition, to evaluate the effects of NPC disease on cellular injury induced by HPBCD, we examined the effects of NPC1 inhibition by gene deletion and pharmacological inhibition using U18666A on the HPBCD-induced cell injury in *in vitro* cultured cells.

2. Material and methods

2.1. Reagents

HPBCD was kindly donated by Nihon Shokuhin Kako Co., Ltd. (Tokyo, Japan). Mayer's hematoxylin, 1% eosin alcohol solution, and mounting medium for histological examination (malinol) were from MUTO Pure Chemicals (Tokyo, Japan). Dulbecco's modified Eagle's medium and F-12 medium were obtained from Gibco-Life Technologies (Life Technologies Japan, Tokyo, Japan). HyClone™ fetal bovine serum (FBS) was purchased from Thermo Scientific (Logan, UT, USA). The cell counting kit and Cellstain® Double Staining Kit were obtained from Dojindo Laboratories (Kumamoto, Japan). All other reagents and solvents were of reagent grade. De-ionized and distilled bio-pure grade water was used throughout the study.

2.2. Animal experiments

Age-matched (9–11 weeks) male wild-type (*Npc1*$^{+/+}$) mice and homozygous (*Npc1*$^{-/-}$) and heterozygous (*Npc1*$^{+/-}$) mutant (BALB/cNctr-*Npc1*^{m1N}) mice [10] were used. A total of 75 mice were used in this study, 35